studies and was directly observed in the neutron crystal structure analysis of oxymyoglobin.[60] Furthermore, the influence of hydrogen bonding to the dioxygen on the O_2 affinity of model systems, such as cobalt Schiff base complexes[55] and "picket-fence" iron porphyrins[61] has been clearly established.

In the crystal structure of $B_{12r}O_2$ (2), both O_α and O_β are involved in hydrogen bonding interactions. The observation of these two hydrogen bonds is also consistent with the description of $B_{12r}O_2$ (2) as superoxocobalamin, which predicts a considerable charge transfer onto the dioxygen ligand.

Acknowledgment. We thank Dr. Arthur Schweiger, ETH Zürich, for helpful discussions. Financial support from the Swiss and Austrian National Science Foundations is acknowledged.

Supplementary Material Available: X-ray structural data for superoxocobalamin ($B_{12r}O_2$, 2), including tables of atomic coordinates, anisotropic and isotropic atomic displacement parameters, bond lengths, bond angles, torsion angles, and hydrogen-bonding distances and figures showing a normal probability plot of the differences in the z coordinates of 2 and 1 for the atoms of the corrin ring and a section through the benzimidazole plane of the final difference Fourier synthesis (11 pages). Ordering information is given on any current masterhead page.

(57) (a) Tsubaki, M.; Yu, N. T. *Proc. Natl. Acad. Sci.* U.S.A. **1981**, *78*, 3581. (b) Kitagawa, T.; Ondrias, M. R.; Rousseau, D. L.; Ikeda-Saito, M.; Yonetani, T. *Nature (London)* **1982**, *298*, 869. (c) Bajdor, K.; Kincaid, J. R.; Nakamoto, K. *J. Am. Chem. Soc.* **1984**, *106*, 7741.
(58) Mims, M. P.; Porras, A. G.; Olson, J. S.; Noble, R. W.; Peterson, J. A. *J. Biol. Chem.* **1983**, *258*, 14219.
(59) (a) Yonetani, T.; Yamamoto, H.; Iizuka, T. *J. Mol. Biol.* **1974**, *249*, 2168. (b) Ikeda-Saito, M.; Iizuka, T.; Yamamoto, H.; Kayne, F. J.; Yonetani, T. *J. Biol. Chem.* **1977**, 252, 4882. (c) Walker, F. A.; Bowen, J. *J. Am. Chem. Soc.* **1985**, *107*, 7632.
(60) Philips, S. E. V.; Schoenborn, B. P. *Nature (London)* **1981**, *292*, 81.
(61) Jameson, G. B.; Drago, R. S. *J. Am. Chem. Soc.* **1985**, *107*, 3017.

Keto-Enol Tautomerization in Metal-Acyl Complexes: The Enolization Properties of Bimetallic μ-Malonyl Compounds

Joseph M. O'Connor,*,†,[1a] Roger Uhrhammer,[1a] Arnold L. Rheingold,*,[1b] and Dean M. Roddick*,[1c]

Contribution from the Departments of Chemistry, University of California at San Diego, La Jolla, California 92093-0506, University of Delaware, Newark, Delaware 19716, and University of Wyoming, Laramie, Wyoming 82071. *Received October 22, 1990*

Abstract: In THF solution, $(\eta^5\text{-}C_5Me_5)(NO)(PPh_3)Re[\mu\text{-}(COCH_2CO)\text{-}C^1,O^3\text{:}C^3]Re(CO)_4$ (2-Re) exists in equilibrium with its enol tautomer $(\eta^5\text{-}C_5Me_5)(NO)(PPh_3)Re\{\mu\text{-}[COCH{=}C(OH)]\text{-}C^1,O^3\text{:}C^3\}Re(CO)_4$ (2-Re-OH), with $K_{eq}^{23°C}$ = [2-Re-OH]/[2-Re] = 0.66. The enol form of the manganese analogue $(\eta^5\text{-}C_5Me_5)(NO)(PPh_3)Re[\mu\text{-}(COCH_2CO)\text{-}C^1,O^3\text{:}C^3]Mn(CO)_4$ (2-Mn) is not observed by NMR spectroscopy in THF. When the enolate anion, $(\eta^5\text{-}C_5Me_5)(NO)(PPh_3)Re\{\mu\text{-}[COCH{=}C(OLi)\text{-}C^1,O^3\text{:}C^3\}Mn(CO)_4$ (2-Mn-OLi) is protonated at low temperature, 2-Mn-OH is generated and completely converted to 2-Mn at room temperature, $K_{eq}^{23°C}$ = [2-Mn-OH]/[2-Mn] <0.02. Both 2-Re and 2-Mn undergo stereoselective exchange of the malonyl ligand hydrogens with deuterium in D_2O. The equilibrium acidity of 2-Re was determined by measuring the ratio of 2-Re to 2-Re-OLi when THF solutions of 2-Re-OLi were treated with 1 equiv of methyl acetoacetate (complete conversion to 2-Re), dimethyl malonate (59% conversion to 2-Re), or methanol (no conversion to 2-Re). The thermodynamic acidity of 2-Re is therefore similar to that of dimethyl malonate in THF. When THF solutions of 2-Re-OLi were treated with 2-Mn, the microscopic acidity of 2-Re was determined to be greater than that of 2-Mn with K = [2-Re-OLi][2-Mn]/[2-Re][2-Mn-OLi] = 80 at −80 °C. The trimethylsilyl enol ethers $(\eta^5\text{-}C_5Me_5)(NO)(PPh_3)Re\{\mu\text{-}[COCH{=}C(OSi(CH_3)_3)]\text{-}C^1,O^3\text{:}C^3\}M(CO)_4$ (2-Re-OSi, M = Re and 2-Mn-OSi, M = Mn) were prepared and structurally characterized as models for 2-Re-OH and 2-Mn-OH. A comparison of the solid-state structures for 2-Re, 2-Mn, 2-Re-OSi, and 2-Mn-OSi indicates that the metallafuran rings in 2-Mn-OH and 2-Re-OH are not significantly aromatic in character. 2-Mn-OSi undergoes hydrolysis in wet THF-d_8 17 times faster than does 2-Re-OSi. The first nonchelating μ-malonyl complex $(\eta^5\text{-}C_5Me_5)(NO)(PPh_3)Re[\mu\text{-}(COCH_2CO)\text{-}C^1\text{:}C^3]Re(CO)_4(PMe_3)$ (5) was prepared by lithium ion abstraction from $\{(\eta^5\text{-}C_5Me_5)(NO)(PPh_3)Re[\mu\text{-}(COCH_2CO)\text{-}C^1\text{:}C^3]Re(CO)_4(PMe_3)\}\cdot Li^+OSO_2CF_3^-$ (4) with 211-kryptofix. In THF 5 exists in equilibrium with its enol tautomer, $(\eta^5\text{-}C_5Me_5)(NO)(PPh_3)Re\{\mu\text{-}[COCH{=}C(OH)]\text{-}C^1\text{:}C^3\}Re(CO)_4(PMe_3)$ (5-OH), with K_{eq} = [5-OH]/[5] = 0.65. The X-ray structures of 5 and 5-OH were determined.

Introduction

The properties and reactivity of organic carbonyl compounds are strongly influenced by keto-enol tautomerization.[2] For example, enols are key intermediates in aldol condensations, electrophilic substitution in carbonyl compounds, and a number of important molecular rearrangements.[3] It is therefore quite striking that, until the work reported here, the enol form of metal-acyl complexes had yet to be observed under conditions of equilibrium with the keto tautomer.[4,5] It is to be expected that access to enolization phenomena in metal acyls will further expand the reactivity manifold available to this important compound class. In organic systems the enol form is often observable and may even be the favored tautomer when the enol is conjugated with an unsaturated substitutent. Furthermore, 1,3-dicarbonyls provide

† Address correspondence to this author at Department of Chemistry, University of Nevada, Reno, NV 89557.

(1) (a) University of California, San Diego. (b) University of Delaware. (c) University of Wyoming.
(2) (a) Forsen, S.; Nilsson, M. In *The Chemistry of the Carbonyl Group, II*; Patai, S., Ed.; Wiley Interscience: New York, 1970. (b) Zimmerman, H. E. *Acc. Chem. Res.* **1987**, *20*, 263 and references therein. (c) Nadler, E. B.; Rappoport, Z.; Arad, D.; Apeloig, Y. *J. Am. Chem. Soc.* **1987**, *109*, 7873 and references therein. (d) Hine, J.; Miles, D. E.; Zeigler, J. P. *J. Am. Chem. Soc.* **1983**, *105*, 4374. (e) Hine, J. *Acc. Chem. Res.* **1978**, *11*, 1. (f) Capon, B.; Siddhanta, A. K.; Zucco, C. *J. Org. Chem.* **1985**, *50*, 3580. (g) Kresge, A. J. *Acc. Chem. Res.* **1990**, *23*, 43.
(3) (a) House, H. O. *Modern Synthetic Reactions*, 2nd ed.; Benjamin: Menlo Park, 1972; pp 629-733, 459-461. (b) Berson, J. A.; Jones, M., Jr. *J. Am. Chem. Soc.* **1964**, *86*, 5019. (c) Conia, J. M.; LePerchec, P. *Synthesis* **1975**, 1. (d) Cookson, R. C.; Parsons, P. J. *J. Chem. Soc., Chem. Commun.* **1976**, 990.

0002-7863/91/1513-4530$02.50/0

Scheme I

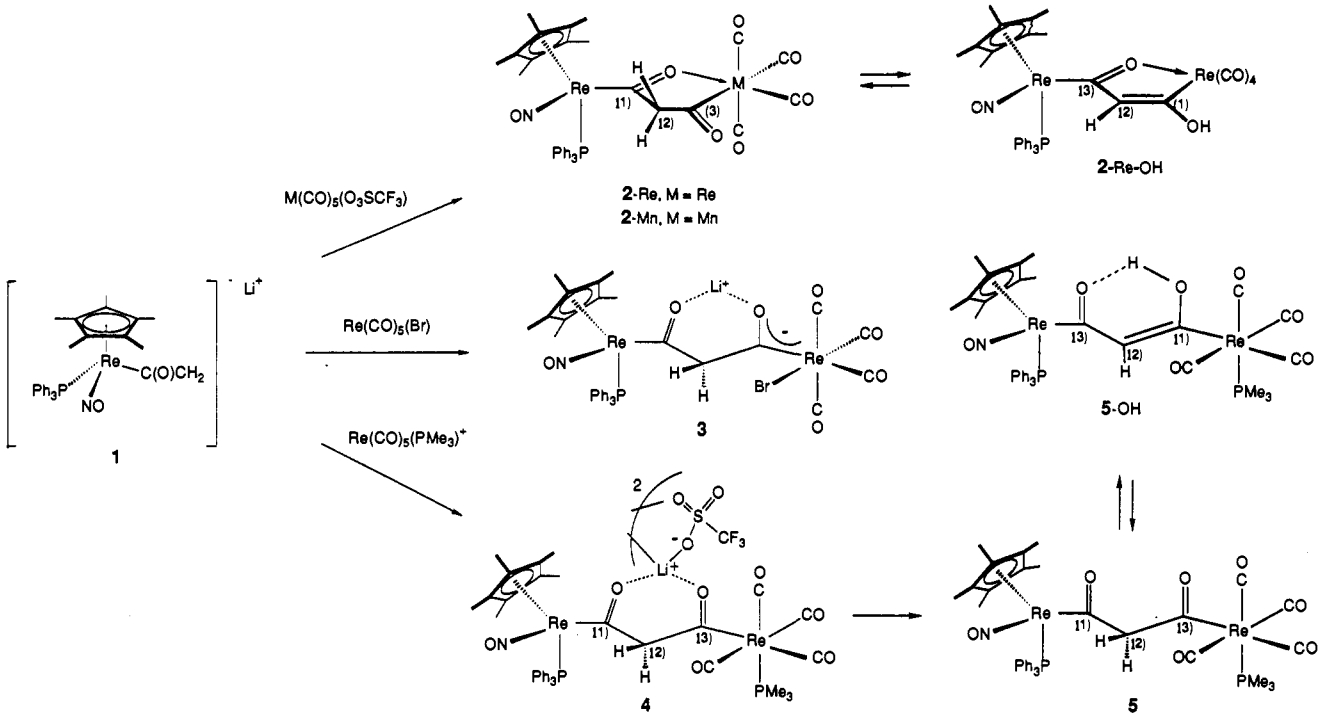

for additional stabilization of the enol tautomer from internal hydrogen bonding. We recently reported the preparation of a subclass of metal–acyl complexes which contain a 1,3–dicarbonyl bridge between two transition metals.[6a] Reaction of (η^5-C_5Me_5)(PPh_3)(NO)Re($COCH_2Li$) (**1**)[7] with metal carbonyl electrophiles led to formation of the μ-malonyl complexes (η^5-C_5Me_5)(NO)(PPh_3)Re[μ-($COCH_2CO$)-C^1,O^3:C^3]M(CO)$_4$ (**2**-M, M = Re, Mn),[6a] {(η^5-C_5Me_5)(NO)(PPh_3)Re[μ-($COCH_2CO$)-C^1:C^3]Re(CO)$_4$(Br)}$^-$Li$^+$ (**3**),[6b] and {(η^5-C_5Me_5)(NO)(PPh_3)Re-[μ-($COCH_2CO$)-C^1:C^3]Re(CO)$_4$(PMe_3)}·Li$^+$$OSO_2CF_3^-$ (**4**)[6c] (Scheme I). Here we report our detailed findings concerning keto–enol tautomerization in bimetallic μ-malonyl complexes including (1) the first direct observations of enol complexes under conditions of equilibrium with a metal–acyl tautomer (**2**-Re/**2**-Re-OH); (2) isotope exchange studies which indicate stereoselective enolization in both **2**-Re and **2**-Mn; (3) determination of the relative acidity of **2**-Re and **2**-Mn; (4) the conversion of **2**-Re and **2**-Mn to the silyl enol ether derivatives (η^5-C_5Me_5)(NO)-(PPh_3)Re{μ-[COCH=C(OSi(CH_3)$_3$)]-C^1,O^3:C^3}M(CO)$_4$ (**2**-Re-OSi, M = Re and **2**-Mn-OSi, M = Mn), and subsequent hydrolysis chemistry; (5) the synthesis and enolization chemistry of the first nonchelating μ-malonyl complex, (C^5-C_5Me_5)-(NO)(PPh_3)Re[μ-($COCH_2CO$)-C^1:C^3]Re(CO)$_4$(PMe_3) (**5**); and (6) the solid-state structures of **2**-Re-OSi, **2**-Mn-OSi, **5**, and the enol tautomer, **5**-OH (Scheme I). Portions of this study have appeared in preliminary form.[6]

Chart I

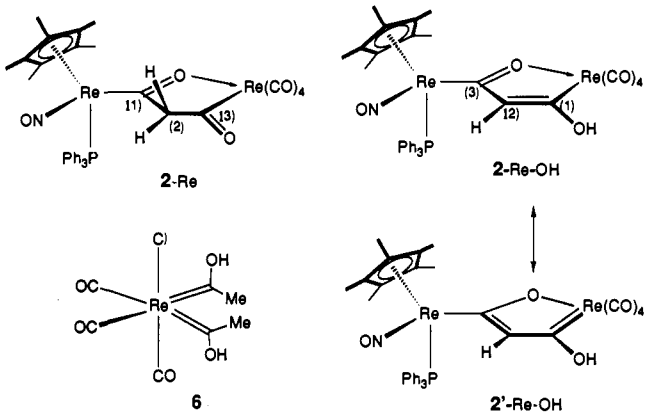

Results

1. Keto–Enol Tautomerization in (η^5-C_5Me_5)(NO)(PPh_3)Re[μ-($COCH_2CO$)-C^1,O^3:C^3]Re(CO)$_4$ (2-Re). The preparation of

(4) (a) Collman, J. P.; Hegedus, L. S.; Norton, J. R.; Finke, R. G. *Principles and Applications of Organotransition Metal Chemistry*; University Science Books: Mill Valley, CA, 1987. (b) Crocco, G. L.; Gladysz, J. A. *J. Am. Chem. Soc.* **1985**, *107*, 4103 and references therein. (c) Liebeskind, L. S.; Welker, M. E.; Fengl, R. W. *J. Am. Chem. Soc.* **1986**, *108*, 6328 and references therein. (d) Davies, S. G. *Pure Appl. Chem.* **1988**, *60*, 13 and references therein. (e) Brookhart, M.; Liu, Y. *Organometallics* **1989**, *8*, 1572 and references therein.

(5) For examples of enol ligands, see: (a) Wakatsuki, Y.; Nozakura, S.; Murahashi, S. *Bull. Chem. Soc. Jpn.* **1971**, *44*, 786–791. (b) Tsutsui, M.; Ori, M.; Francis, J. *J. Am. Chem. Soc.* **1972**, *94*, 1414. (c) Brookhart, M.; Harris, D. *J. Org. Chem.* **1972**, *42*, 441–446. (d) Thyret, H. *Angew Chem., Int. Ed. Engl.* **1972**, *11*, 520–521. (e) Cotton, F. A.; Francis, J. N.; Frenz, B. A.; Tsutsui, M. *J. Am. Chem. Soc.* **1973**, *95*, 2483–2486. (f) Hillis, J.; Tsutsui, M. *J. Am. Chem. Soc.* **1973**, *95*, 7907–7908. (g) Francis, J.; Tsutsui, M. *Chem. Lett.* **1973**, 663–664. (h) Hillis, J.; Francis, J.; Ori, M.; Tsutsui, M. *J. Am. Chem. Soc.* **1974**, *96*, 4800–4804. (i) Cutler, A.; Raghu, S.; Rosenblum, M. *J. Org. Chem.* **1974**, *77*, 381–391. (j) Kanda, Z.; Nakamura, Y. Kawaguchi, S. *Chem. Lett.* **1976**, 199–200. (k) White, C.; Thompson, S. J.; Maitlis, P. M. *J. Org. Chem.* **1977**, *134*, 319–325. (l) Kanda, Z.; Nakamura, Y.; Kawaguchi, S. *Inorg. Chem.* **1978**, *17*, 910–914. (m) Fairhurst, G.; White, C. *J. Chem. Soc., Dalton Trans.* **1979**, 1531–1538. (n) Roustan, J. L.; Guinot, A.; Cadiot, P. *J. Org. Chem.* **1980**, *194*, 191–202. (o) Effenberger, F.; Keil, M. *Tetrahedron Lett.* **1981**, *22*, 2151–2154. (p) McCrindle, R.; Perguson, G.; McAlees, A. J.; Ruhn, B. L. *J. Org. Chem.* **1981**, *204*, 273–279. (q) Casey, C. P.; O'Connor, J. M.; Haller, K. J. *J. Am. Chem. Soc.* **1985**, *107*, 3172–3177. (r) Vollhardt, K. P. C.; Wolfgruber, M. *Angew. Chem., Int. Ed. Engl.* **1986**, *25*, 929–931. (s) Suggs, J. W.; Wovkulich, M. J.; Williard, P. G.; Lee, K. S. *J. Org. Chem.* **1986**, *307*, 71–82. (t) Fornals, D.; Perricàs, M. A.; Serratosa, F.; Vinaixa, J.; Font-Altaba, M.; Solans, X. *J. Chem. Soc., Perkin Trans. 1* **1987**, 2749–2752. (u) Bodner, G. S.; Smith, D. E.; Hatton, W. G.; Heah, P. C.; Georgiou, S.; Rheingold, A. L.; Geib, S. J.; Hutchinson, J. P.; Gladysz, J. A. *J. Am. Chem. Soc.* **1987**, *109*, 7688–7705. (v) Harman, W. D.; Dobson, J. C.; Taube, H. *J. Am. Chem. Soc.* **1989**, *111*, 3061–3062.

(6) (a) O'Connor, J. M.; Uhrhammer, R.; Rheingold, A. L. *Organometallics* **1987**, *6*, 1987. (b) O'Connor, J. M.; Uhrhammer, R.; Rheingold, A. L.; Staley, S. L.; Chadha, R. K. *J. Am. Chem. Soc.* **1990**, *112*, 7585. (c) O'Connor, J. M.; Uhrhammer, R.; Rheingold, A. L.; Staley, D. L. *J. Am. Chem. Soc.* **1989**, *111*, 7633. (d) O'Connor, J. M.; Uhrhammer, R. *J. Am. Chem. Soc.* **1988**, *110*, 4448. (e) O'Connor, J. M.; Uhrhammer, R.; Rheingold, A. L. *Organometallics* **1988**, *7*, 2422.

(7) Heah, P. C.; Patton, A. T.; Gladysz, J. A. *J. Am. Chem. Soc.* **1986**, *108*, 1185.

Scheme II

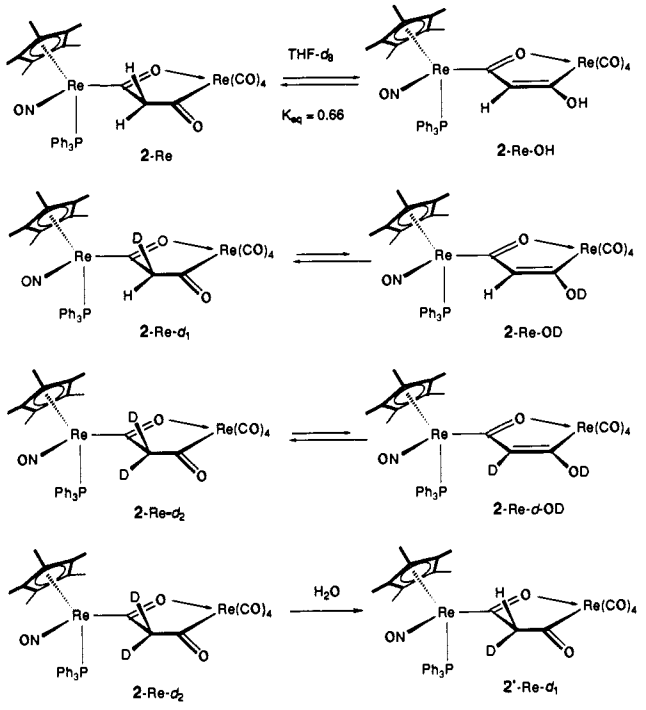

2-M (M = Re, Mn)[6a] from rhenaenolate **1**[7] and $M(CO)_5(OSO_2CF_3)$ has led to the first direct observation of keto–enol tautomerization in metal–acyl complexes. In halogenated solvents such as chloroform or methylene chloride there was no spectroscopic evidence for the enol form of **2**-Re or **2**-Mn, even in the presence of added water. However, in THF-d_8, the enol complex, $(\eta^5\text{-}C_5Me_5)(NO)(PPh_3)Re[\mu\text{-}[COCH{=}C(OH)]\text{-}C^1,O^3{:}C^3]Re(CO)_4$ (**2**-OH), was observed in equilibrium with **2**-Re ($K_{eq}^{23°C}$ = [**2**-Re-OH]/[**2**-Re] = 0.66). The equilibrium is temperature dependent with $K_{eq}^{-80°C}$ = 2.3. Resonances in the ^1H NMR spectrum at δ 8.91 [s, C(=O)CH=C(O*H*)], 6.28 [s, C(=O)-C*H*=C(OH)], and 1.73 [s, $C_5(CH_3)_5$] were attributed to the enol complex **2**-Re-OH (Table I). In the ^{31}P NMR spectrum, two phosphorus resonances were observed at δ 19.4 (**2**-Re) and 22.7 (**2**-Re-OH) in a ~2.1 ratio. When the THF solvent was replaced with $CDCl_3$, only the resonances due to **2**-Re were observed, indicating a shift of the equilibrium toward the keto form. Relative to halogenated solvents, THF is expected to stabilize the enol form by functioning as a hydrogen bond acceptor.[8] Even when the THF-d_8 was rigorously dried and the NMR tube previously flame-dried under high vacuum, the keto–enol equilibrium was observed in the ^1H NMR spectrum of **2**-Re.

A hydroxycarbene structure; **2'**-Re-OH, is also a possibility for the observed enol complex; however, such a structure is expected to exhibit a downfield carbene carbon resonance in the ^{13}C NMR spectrum (Chart I). For example, the hydroxycarbene $Re(CO)_3(Cl)[{=}CMe(OH)]_2$ (**6**, Chart I) has a carbene carbon chemical shift of 322.2 ppm in the ^{13}C NMR spectrum.[9] The isotopically enriched complex $(\eta^5\text{-}C_5Me_5)Re(NO)(PPh_3)\{\mu\text{-}[COCH{=}^{13}C(OH)]C^1,O^3{:}C^3\}Re(^{13}CO)_4$ exhibits a *C*OH carbon resonance at 225.4 ppm in the ^{13}C NMR spectrum. This value is consistent with some carbenoid character and therefore indicates a minor resonance contribution from the hydroxycarbene structure **2'**-Re-OH (X-ray data, vide infra).

By following the exchange of the methylene hydrogens with D_2O in THF-d_8 solvent, it is clear that the keto–enol tautomerization in **2**-Re is a kinetic stereoselective process.[10] When D_2O

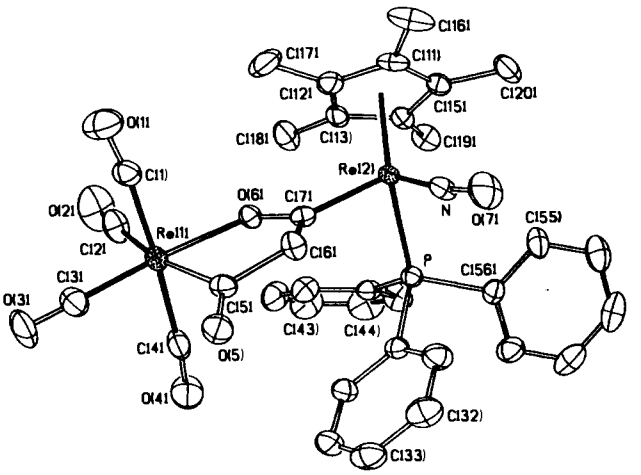

Figure 1. Structure of $(\eta^5\text{-}C_5Me_5)(NO)(PPh_3)Re[\mu\text{-}(COCH_2CO)\text{-}C^1,O^3{:}C^3]Re(CO)_4$ (**2**-Re).

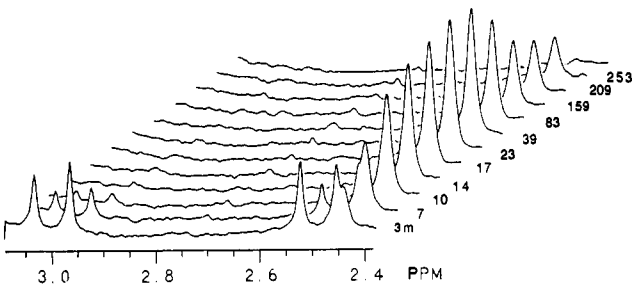

Figure 2. Time course of deuterium incorporation from D_2O into the methylene hydrogen sites of **2**-Re as observed by ^1H NMR spectroscopy.

(2.1 M) was added to an NMR tube containing a THF-d_8 solution of **2**-Re (4.0 M) in equilibrium with **2**-Re-OH (2.6 mM) and the solution was monitored by ^1H NMR spectroscopy, the two methylene hydrogens of the malonyl ligand were observed to incorporate deuterium at different rates (Scheme II). Three minutes after addition of D_2O, a ^1H NMR spectrum of the sample indicated complete exchange of deuterium into the hydroxyl site (δ 8.91) to give **2**-Re-OD. There was no evidence for exchange into the vinyl hydrogen position (δ 6.28). In addition to the methylene hydrogen resonances of **2**-Re at δ 2.49 (d, J = 20.5 H) and 3.00 (d, J = 20.5 Hz), a new broad singlet was observed in the methylene region at 2.44 ($\nu_{1/2}$ = 6 Hz).[11] The 6-Hz bandwidth is consistent with $J_{HD} \approx 3$ Hz.[12] We assign the new

(8) Reichardt, C. *Solvent Effects in Organic Chemistry*; Verlag Chemie: New York, 1979; Chapter 4.

(9) Darst, K. P.; Lenhert, P. G.; Lukehart, C. M.; Warfield, L. T. *J. Organomet. Chem.* **1980**, *195*, 317.

(10) For examples of stereoselective hydrogen–deuterium exchange in organic systems, see: Peiris, S.; Ragauskas, A. J.; Stothers, J. B. *Can. J. Chem.* **1987**, *65*, 789. Keys III, L. D.; Johnston, M. *J. Am. Chem. Soc.* **1985**, *107*, 486. Cheng, A. K.; Ghosh, A. K.; Stothers, J. B. *Can. J. Chem.* **1984**, *62*, 1385. Wu, G. D.; Serianni, A. S.; Barker, R. *J. Org. Chem.* **1983**, *48*, 1750. Gabioud, R.; Vogel, P. *Tetrahedron Lett.* **1983**, *24*, 1983. Guthrie, R. D.; Nicolas, E. C. *J. Am. Chem. Soc.* **1981**, *103*, 4637. Fraser, R. R.; Champagne, P. J. *J. Am. Chem. Soc.* **1978**, *100*, 657 and references therein. Barbarella, G.; Garbesi, A.; Fava, A. *J. Am. Chem. Soc.* **1975**, *97*, 5883 and references therein. King, J. F.; DuManoir, J. R. *Can. J. Chem.* **1973**, *51*, 4082. Hofer, O.; Eliel, E. L. *J. Am. Chem. Soc.* **1973**, *95*, 8045. Eliel, E. L. *Angew. Chem., Int. Ed. Engl.* **1972**, *11*, 748. Hutchinson, B. J.; Andersen, K. K.; Katritzky, R. *J. Am. Chem. Soc.* **1969**, *91*, 3839. Bullock, E.; Scott, J. M.; Golding, P. D. *J. Chem. Soc., Chem. Commun.* **1967**, 168. Nishio, M. *J. Chem. Soc., Chem. Commun.* **1967**, 562. Rauk, A.; Buncel, E.; Moir, R. T.; Wolfe, S. *J. Am. Chem. Soc.* **1965**, *87*, 5498. Fukunaga, M.; Arai, K.; Iwamura, H.; Oki, M. *Bull. Chem. Soc. Jpn.* **1972**, *45*, 302. Saito, H.; Matsuo, T. *Nippon Kagaku Kaishi* **1979**, *12*, 1720.

(11) (a) Isotope chemical shift effects resulting from substitution of a deuterium atom for a methylene hydrogen atom generally lead to an upfield shift of ~0.01 to 0.03 ppm in the ^1H NMR spectrum: Batiz-Hernandez, H., Bernheim, R. A. *Prog. Nucl. Magn. Reson. Spectrosc.* **1967**, *3*, 63. Barras, C. A.; Roulet, R.; Carrupt, P.-A.; Berchier, F.; Vogel, P. *Helv. Chim. Acta* **1984**, *67*, 886. Golding, B. T.; Ioannou, P. V.; Sellers, P. *J. Inorg. Chim. Acta* **1981**, *56*, 95. Sakaguchi, U.; Morito, K.; Yoneda, H. *J. Am. Chem. Soc.* **1979**, *101*, 2767. (b) The ^1H NMR isotope chemical shifts observed for **2**-Re-d_1 (0.05 ppm) and **2**-Mn-d_1 (0.04 ppm) are larger than expected and may not represent the intrinsic isotope shift value.

Table I. ^1H and ^{13}C NMR Characterization of Enol, Silyl Ether, and Enolate Complexes

complex[a]	^1H NMR,[b] δ		$^{13}C\{^1H\}$ NMR,[c] ppm	
	ReC(O)C*H*=C(OX)M	ReC(O)CH=C(O*X*)M	ReC(O)CH=C(OX)M	ReC(O)CH=C(OX)M
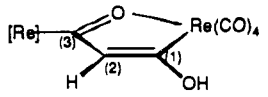 **2**-Re-OH	(X = H) 6.28 (s)	(X = H) 8.91 (s)	(X = H) 270.3 (d, J = 8.5) (−80°)	(X = H) 225.4 224.0 (−80°)
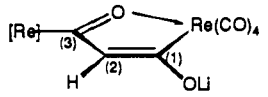 **2**-Re-OLi	(X = Li) 5.98 (br s)	(X = Li)	(X = Li) not obsd	(X = Li) 250.0 (45°)
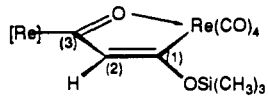 **2**-Re-OSi	[X = $Si(CH_3)_3$] 6.47 (s)	[X = $Si(CH_3)_3$] 0.27	[X = $Si(CH_3)_3$] 272.6 (d, J = 11 Hz)	[X = $Si(CH_3)_3$] 223.6
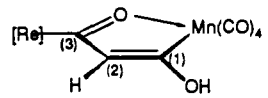 **2**-Mn-OH	(X = H) 6.13 (s) (−80°)	(X = H) 9.62 (s) (−80°)	(X = H)	(X = H)

complex	^1H NMR, δ		$^{13}C\{^1H\}$ NMR, ppm	
	ReC(O)C*H*=C(OH)M	ReC(O)CH=C(O*X*)M	ReC(O)CH=C(OH)M	ReC(O)CH=C(OX)M
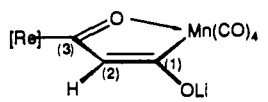 **2**-Mn-OLi	(X = Li) 5.79 (br s, $\nu_{1/2}$ = 40 Hz)	(X = Li)	(X = Li) 246.2 (br m) or 254.1 (br m) (45°)	(X = Li) 254.1 (br m) or 246.2 (br m) (45°)
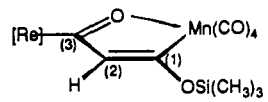 **2**-Mn-OSi	[X = $Si(CH_3)_3$] 6.36	[X = $Si(CH_3)_3$] 0.28	[X = $Si(CH_3)_3$] 268.2 (d, J = 9.3 Hz)	[X = $Si(CH_3)_3$] 237.8
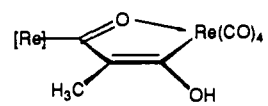 **7**-OH	ReC(O)C(CH_3)=C(OH)M 1.97 (s, 3 H)	(X = H) 8.92 (s, 1 H)	(X = H) 279.1 (d, J = 9.1 Hz)	(X = H) 219.3
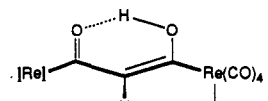 **5**-OH	(X = H) 6.10 (s)	(X = H) 16.44 (s)	(X = H) 249.3 (d, J = 9.2 Hz)	(X = H) one of the resonances between 189 and 195

[a] [Re] ≡ $Re(PPh_3)(NO)(C_5(CH_3)_5)$. [b] ^1H NMR spectra were recorded at 300 or 500 MHz in THF-d_8 at ambient probe temperature (unless otherwise stated) and were referenced to the residual solvent resonance at δ 1.73 or 3.58. [c] ^{13}C NMR spectra were recorded at 75 or 126 MHz in THF-d_8 at ambient probe temperature (unless otherwise indicated) and were referenced to the solvent resonance at 67.4 ppm.

resonance at δ 2.44 to **2**-Re-d_1 in which deuterium occupies the methylene site exo to the PPh_3 ligand, when the molecule occupies the favored conformation with a ON–Re–C_α–O torsion angle of ~180° (Figure 1).[13] Rapid ($t_{1/2} \approx$ 3–4 min) deuterium incorporation into **2**-Re was observed as a decrease in the peak height of the δ 2.49 and 3.00 doublets and a corresponding increase in the 2.44 resonance (Figure 2). Exchange into the remaining methylene site (H-endo) was observed as a decrease in the peak height of the broad δ 2.44 resonance ($t_{1/2} \approx$ 120 min). The exo hydrogen therefore underwent exchange ~30 times faster than the endo hydrogen. In a separate experiment, **2**-Re (22.2 mM) and D_2O (3.8 M) underwent exchange at a significantly slower rate, with $t_{1/2} \approx$ 10 min for the exo hydrogen and $t_{1/2} \approx$ 3.6 h for the endo hydrogen. In this sample the exo hydrogen underwent deuterium exchange ~20 times faster than the endo hydrogen. The rate differences in the two experiments may be due to the presence of adventitious acid or base.

The assignment of exo and endo hydrogens in **2**-Re is consistent with shielding of the endo hydrogen by the phenyl substituents on phosphorus and the solid-state structures of **2**-Re (Figure 1)[6b] and **2**-Mn.[6a] The assignment is also supported by the results of NOE experiments. In the ^1H NMR spectrum (500 MHz) of **2**-Re, saturation of the δ 7.30 (m, 3 C_6H_5) resonance led to a 4.6% increase in the δ 2.49 doublet and an insignificant decrease in the δ 3.00 doublet. Saturation of the δ 1.76 [s, $C_5(CH_3)_5$] resonance resulted in a barely perceptible decrease in the upfield doublet at δ 2.49 and a 1.3% increase in the downfield doublet at δ 3.00. It was not possible to selectively saturate the δ 2.49 or 3.00 signals due to the line width (J = 20.5 Hz).

Consistent with the above chemical shift assignments is the spectroscopic observation of the alternative d_1 isomer, **2'**-Re-d_1, when H_2O was added to a CD_2Cl_2 solution of **2**-Re-d_2 (Scheme II). In the ^1H NMR spectrum of the sample, a transient resonance

(12) Bovey, F. A.; Jelinski, L.; Mirau, P. A. *Nuclear Magnetic Resonance Spectroscopy*; Academic Press: New York, 1988; p 193.

(13) For a detailed discussion on ON–Re–C_αO torsion angles and asymmetric induction in (η^5-C_5H_5)Re(NO)(PPh_3)(R) complexes, see: Bodner, G. S.; Smith, D. E.; Hatton, W. G.; Heah, P. C.; Georgiou, S.; Rheingold, A. L.; Geib, S. J.; Hutchinson, J. P.; Gladysz, J. A. *J. Am. Chem. Soc.* **1987**, *109*, 7688 and references therein.

Scheme III

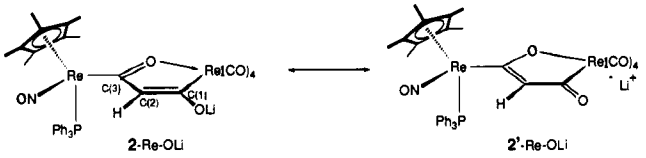

was observed at δ 3.03, which is 0.04 ppm to higher field from the 3.07 doublet of **2**-Re in CD_2Cl_2. We therefore assign the δ 3.03 resonance to the *exo*-methylene hydrogen in **2'**-Re-d_1.

2. Generation of $(\eta^5$-$C_5Me_5)(NO)(PPh_3)Re\{\mu$-[COCH=C(OLi)]-$C^1,O^3:C^3\}Re(CO)_4$ (2-Re-OLi). Deprotonation of **2**-Re (39.2 mg, 0.03 mmol, 43.8 mM) with *t*-BuOLi (3.2 mg, 0.04 mmol) in THF-d_8 generates the enolate anion, **2**-Re-OLi, as determined by NMR spectroscopy. In the ^1H NMR spectrum, resonances attributed to **2**-Re-OLi were observed at δ 1.72 (s, overlap with THF-d_7 signal), 5.98 (br s, 1 H), 7.32 and 7.54 (br s, 15 H). In addition, *t*-BuOH resonances were observed at δ 1.14 and 3.19. In the ^{13}C NMR spectrum of the isotopically enriched enolate complex $(\eta^5$-$C_5Me_5)(NO)(PPh_3)Re\{\mu$-[COCH=^{13}C(OLi)]-$C^1,O^3:C^3\}Re(^{13}CO)_4$, C^1 was observed at 250 ppm. This value is between that observed for the related carbon atom in **2**-Re (C^3, 275.6 ppm) and **2**-Re-OH (C^1, 225.4) and indicates a degree of acyl character at that carbon in **2**-Re-OLi, as shown for resonance structure **2'**-Re-OLi (Scheme III).

From the IR spectrum of isolated **2**-Re-OLi it is clear that the negative charge resides to a significant extent at the two metal centers in addition to the oxygen atom. The carbonyl and nitrosyl stretching bands are shifted to lower wavenumber [KBr 2060 (m), 1942 (s, br), 1895 (s) 1631 cm^{-1}] on going from **2**-Re to **2**-Re-OLi. The shift of ν(NO) from 1664 in **2**-Re to 1631 cm^{-1} in **2**-Re-OLi is also consistent with the resonance contributor, **2'**-Re-OLi. A band at 1405 (m) was not observed in the IR spectrum of the labeled isomer, $(\eta^5$-$C_5Me_5)Re(NO)(PPh_3)\{\mu$-[COCH=^{13}C(OLi)]-$C^1,O^3:C^3\}Re(^{13}CO)_4$, and a new broad band was observed at 1370 cm^{-1} (overlapping a 1375 band observed in the spectrum of unlabeled **2**-Re-OLi). We therefore assign the 1405-cm^{-1} stretch to ν(C–OLi).

When **2**-Re-OLi was protonated by CF_3CO_2H in THF-d_8 at −80 °C and the sample was monitored by ^1H NMR spectroscopy, an equilibrium mixture of **2**-Re and **2**-Re-OH was observed; $K_{eq}^{-80°C}$ = [2-Re-OH]/[2-Re] = 2.3. A ^{13}C NMR spectrum of the sample exhibited resonances assigned to **2**-Re-OH at 270.3 (d, J = 8.5 Hz, C^3), 224.0 (C^1), 194.7 (ReCO), 193.3 (ReCO), 191.3 (ReCO), 189.6 (ReCO), 139–128.7 (m, C_6H_5 for both **2**-Re and **2**-Re-OH), 103.2 [$C_5(CH_3)_5$], and 10.1 [$C_5(CH_3)_5$]ppm. In addition to the resonances assigned to **2**-Re and **2**-Re-OH, signals at 161.1 (q, J = 34 H) and 118.0 (q, J = 293 Hz) ppm were asssigned to the carbons of CF_3CO_2Li.

3. Keto-Enol Tautomerization in $(\eta^5$-$C_5Me_5)(NO)(PPh_3)Re$-$[\mu$-$(COCH_2CO)$-$C^1,O^3:C^3]Mn(CO)_4$ (2-Mn). In contrast to **2**-Re, THF-d_8 solutions of the manganese analogue, **2**-Mn, exhibited no ^1H NMR resonances attributable to an enol tautomer ($K_{eq}^{23°C}$ = [2-Mn-OH]/[2-Mn] < 0.02). Attempts to observe the enol form, **2**-Mn-OH, by ^1H NMR spectroscopy in wet THF-d_8 and at low temperature, where the equilibrium favored the enol form in the case of **2**-Re, were unsuccessful. However, addition of D_2O to THF-d_8 solutions of **2**-Mn resulted in different rates of deuterium incorporation into the *exo*- and *endo*-methylene hyrogen sites; an indication that keto–enol tautomerization may also be occurring in **2**-Mn, with the equilibrium lying far to the side of the keto form (Scheme IV). The ^1H NMR spectrum of **2**-Mn (11 mg, 0.02 M) in THF-d_8 exhibited resonances at δ 1.79 (s, 15 H), 2.81 (d, J = 20 Hz, 1 H), 3.36 (d, J = 20 Hz, 1 H), and 7.4 (m, 15 H). When D_2O (47 μL, 4.10 M) was added to the sample, the residual HOD resonance was observed at δ 3.38 as a broad singlet which partially obscured the low field line of the 3.36 doublet for **2**-Mn. The disappearance of **2**-Mn was then monitored by the decrease in the intensity of the doublet at δ 2.81, and the initial formation of **2**-Mn-d_1 was observed as the appearance of a new broad band at 2.77. After 13 h the methylene resonances

Scheme IV

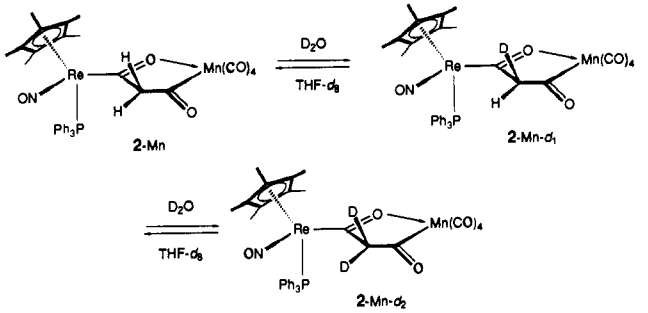

Scheme V

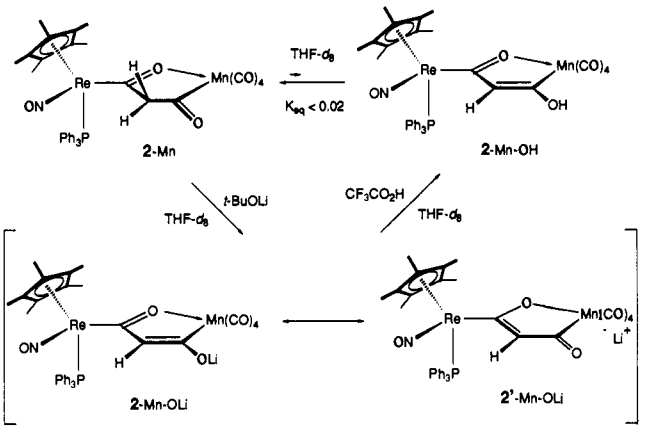

for **2**-Mn were no longer detectable, and the δ 2.77 singlet (**2**-Mn-d_1) had reached 74% of its theoretical maximum intensity ($t_{1/2} \approx$ 200 min). The remaining 26% of the material was presumably **2**-Mn-d_2. Over the course of 4 days, the δ 2.77 resonance slowly decreased in intensity and disappeared into the baseline as **2**-Mn-d_1 was completely converted to **2**-Mn-d_2 ($t_{1/2} \approx$ 36 h). The exo hydrogen therefore undergoes deuterium exchange, and presumably keto–enol tautomerization, ca. eleven times faster than the endo hydrogen. This contrasts with the **2**-Re result in which the rate difference between exo and endo exchange was large enough to see ≥95% formation of **2**-Re-d_1 before detectable conversion to **2**-Re-d_2 occurred.

In an effort to observe the enol form, **2**-Mn-OH, *t*-BuOLi (3.3 mg, 0.04 mmol) was added to a THF-d_8 solution to **2**-Mn (34.9 mg, 0.04 mmol, 44.6 mM) and the ^1H NMR spectrum recorded. Resonances at δ 1.69 (s, 15 H), 5.79 (br s, $\nu_{1/2}$ = 40 Hz, 1 H), and 7.3, 7.52 (br s, 15 H) were attributed to formation of the enolate anion, **2**-Mn-OLi (Scheme V). At 50 °C the broad singlet for the vinyl hydrogen resonance sharpened ($\nu_{1/2}$ = 18 Hz) and at −80 °C three vinyl hydrogen resonances were observed at δ 5.57, 5.96, and 5.99 in a 1:12:4 ratio. The nature of the three vinyl isomers is unknown, although they may be due to lithium aggregates and/or to isomers with different ON–Re–C_α–O torsion angles (e.g., θ = 0° or 180°). In the $^{13}C\{^1H\}$ NMR spectrum of the sample at 45 °C, the carbonyl carbons of the malonate ligand were observed at 254.1 (br m) and 246.2 (v br m) ppm, and the terminal carbonyl ligand resonances were observed at 221.5, 219.8, 219.7, and 216.0. For comparison, the corresponding ^{13}C NMR resonances (CD_2Cl_2) for **2**-Mn were observed at 283.2 (d, J = 10 Hz), 282.3, 219.4, 216.1, 212.6, and 211.8 ppm. The upfield shift of the malonyl ^{13}C NMR resonances from 293 and 282 ppm in **2**-Mn to 254 and 246 in **2**-Mn-OLi is indicative of an increase in electron density at the metal centers, consistent with resonance form **2'**-Mn-OLi. The effect of such a charger distribution is to decrease the degree of carbenoid character at C^1 and C^3 of the bridging ligand.

When the sample was cooled to −78 °C and CF_3CO_2H (3.2 μL, 0.04 mmol) added, ^1H NMR resonances (−80 °C) attributed to **2**-Mn (25.1 mM) were observed at δ 2.58 (d, J = 21.2 Hz) and 3.42 (d, J = 21.6 Hz) and resonances at 6.13 [s, C(=O)-

Scheme VI

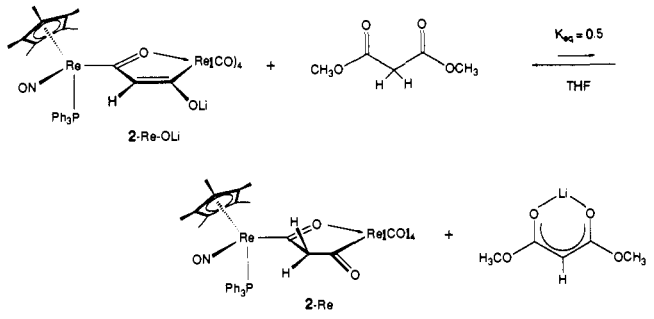

Scheme VII

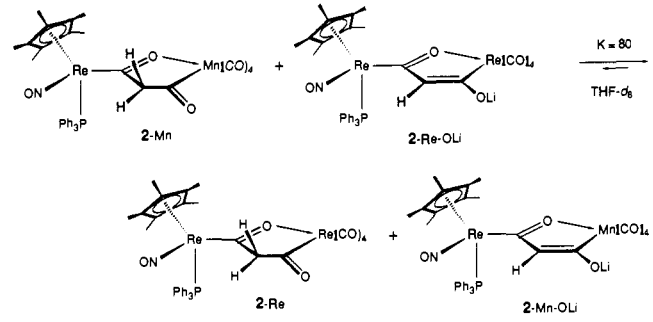

Scheme VIII

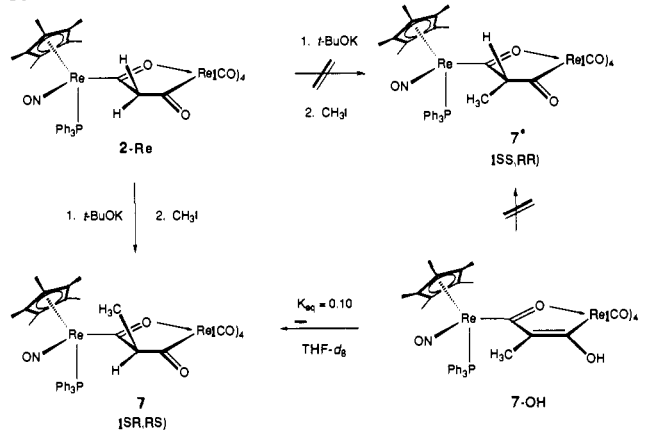

C*H*=C(OH)] and 9.62 [s, C(=O)CH=C(O*H*)] were assigned to **2**-Mn-OH (12.8 mM).[14] In a separate experiment, the half-life for disappearance of **2**-Mn-OH was determined to be <9 min at −80 °C, under similar conditions. At 23 °C, a ^{1}H NMR spectrum of the sample indicated complete conversion of **2**-Mn-OH to **2**-Mn.

In order to determine the relative rates of deuterium incorporation into the methylene hydrogens of **2**-Re and **2**-Mn, a competition experiment was performed. An NMR tube was charged with **2**-Re (16.3 mM) and **2**-Mn (15.7 mM) in THF-d_8. Deuterated water was added (3.6 M), and the sample was monitored by ^{1}H NMR spectroscopy. The relative rate of disappearance of **2**-M was determined to be $k_{Re}/k_{Mn} = 10$, the relative rate of **2**-M-d_1 appearance was $k_{Re}/k_{Mn} = 4$, and the relative rate for disappearance of **2**-M-d_1 was $k_{Re}/k_{Mn} = 6$. The rate of disappearance of **2**-M is faster than the rate of appearance of **2**-M-d_1, due to simultaneous conversion of **2**-M-d_1 to **2**-M-d_2. The exo hydrogen of **2**-Re therefore undergoes enolization ca. ten times faster than for **2**-Mn, whereas the endo hydrogen of **2**-Re enolizes ca. six times faster than for **2**-Mn.

4. Acidity of $(\eta^5$-$C_5Me_5)(NO)(PPh_3)Re[\mu$-$(COCH_2CO)$-$C^1,O^3$:$C^3]M(CO)_4$ (2-M, M = Re, Mn). The equilibrium acidity of **2**-Re was determined by measuring the ratio of malonyl (**2**-Re) to enolate anion (**2**-Re-OLi) when THF solutions of the enolate were treated with methyl acetoacetate, dimethyl malonate, or methanol. In an NMR tube experiment, **2**-Re (19.3 mg, 0.0197 mmol, 39 mM) and *t*-BuOLi (0.0213 mmol, 42 mM) were dissolved in THF-d_8, and the solution was heated briefly at reflux to dissolve the solids. A ^{1}H NMR spectrum of the sample revealed complete conversion of **2**-Re to **2**-Re-OLi [δ 1.72 (s, overlap with THF-d_7 signal), 5.98 (br s, $\nu_{1/2}$ = 12 Hz, 1 H), 7.32 and 7.54 (br s, 15 H)]. Resonances at δ 3.20 (s, 1 H) and 1.14 (s, 9 H) indicated the presence of 1 equiv of *t*-BuOH. In the dry box, 1.1 equiv of methyl acetoacetate (42 mM) was added, and a second ^{1}H NMR spectrum was obtained. Resonances for **2**-Re and **2**-Re-OH were observed at δ 3.01 (d, J = 20.5 Hz), 2.48 (d, J = 20.5 Hz), 1.76 (s), and 9.0 (br m), 6.29 (s), 1.77 (s); with [**2**-Re-OH]/[**2**-Re] = 0.62. Resonances attributed to $[CH_3C(O)CHCO_2CH_3]^-Li^+$ at δ 4.57 (s, 1 H), 3.46 (s, 3 H), 1.80 (s) (38 mM), and $CH_3C(O)CH_2CO_2CH_3$ at 3.64 (s), 3.43 (s), 2.17 (s) (4 mM) were also observed.[14] No signals for **2**-Re-OLi were present. Thus, addition of 1.1 equiv of methyl acetoacetate to a THF solution of **2**-Re-OLi led to essentially 100% protonation of **2**-Re-OLi.

In a related experiment, the enolate anion **2**-Re-OLi was generated in situ (THF-d_8) from **2**-Re (29.5 mM) and *t*-BuOLi (30.7 mM), and 1 equiv of dimethyl malonate (29.1 mM) was added. A ^{1}H NMR spectrum indicated that **2**-Re-OLi was 59% protonated by the organic acid. The microscopic acidity K = [**2**-Re-OLi][$(CO_2CH_3)_2CH_2$]/[**2**-Re][$(CO_2CH_3)_2CHLi$] = 0.5. In a similar fashion, when a THF-d_8 solution of **2**-Re was treated with 1.2 equiv of $[(CO_2CH_3)CH]^-Li^+$, 46% of **2**-Re was deprotonated and, in agreement with the previous experiment, K = [**2**-Re-OLi][$(CO_2CH_3)_2CH_2$]/[**2**-Re][$(CO_2CH_3)_2CHLi$] = 0.5. Under similar conditions, 1 equiv of methanol failed to give measurable protonation of **2**-Re-OLi. The thermodynamic acidity of **2**-Re is therefore similar to that of dimethyl malonate in THF solvent.

On the basis of the keto–enol equilibrium differences observed for **2**-Re and **2**-Mn it was anticipated that **2**-Re would prove to be more acidic than **2**-Mn (Scheme VII). To test this hypothesis an NMR tube experiment was carried out in which **2**-Re-OLi was generated to THF-d_8 by treatment of **2**-Re (0.023 mmol) with *t*-BuOLi (0.0238 mmol, 45.8 mM), in the presence of 1,4-bis(trimethylsilyl)benzene is internal standard. To this heterogeneous solution **2**-Mn (0.023 mmol) was added. The sample was briefly heated at reflux to dissolve the solids, and an ^{1}H NMR spectrum was taken at 23 °C. At this temperature the vinyl resonances were broad. A ^{1}H NMR spectrum of the sample was therefore recorded at −80 °C which exhibited distinct resonances due to **2**-Re (1.5 mM), **2**-Re-OH (1.2 mM), **2**-Re-OLi (21.8 mM), **2**-Mn, (27.7 mM), **2**-Mn-OH (1.5 mM), and **2**-Mn-OLi (5.0 mM).[14] The microscopic acidity of **2**-Re was determined to be greater than that of **2**-Mn, with K = [**2**-Re-OLi][**2**-Mn]/[**2**-Mn-OLi] ≈ 80 at −80°C. To assure that an equilibrium was established under these conditions, a related experiment was performed in which **2**-Mn-OLi and **2**-Re were converted to **2**-Mn and **2**-Re-OLi in nearly quantitative yield.

5. Keto–Enol Tautomerization in $(\eta^5$-$C_5Me_5)(NO)(PPh_3)$Re-$\{\mu$-$[COCH(CH_3)CO]$-C^1,O^3:$C^3\}Re(CO)_4$ (7). In situ deprotonation of **2**-Re with *t*-BuOK and methylation of the resultant anion with CH_3I led to a 91% isolated yield of the C-alkylated product **7** (Scheme VIII). A single-crystal X-ray analysis established the stereochemistry for **7** as *SR,RS*.[6e,15] The complex exhibits a ON–Re–C_α–O torsion angle of 179° as was observed in the solid-state structures of **2**-Re (Figure 1)[6b] and **2**-Mn.[6a] The methyl group is exo to the bulky PPh_3 ligand. As was the case for **2**-Re, the methyl-substituted complex **7** was observed in equilibrium with its enol form **7**-OH, by ^{1}H NMR spectroscopy (THF-d_8). The expected malonyl ligand resonances were observed at δ 1.01 (d, J = 7.9 Hz, 1 H) and 2.07 (q, J = 7.9 Hz, 3 H), and the char-

(14) Errors in mass balance are presumably due to precipitation, particularly in low-temperature experiments. This does not effect the microscopic acidity constant values.

(15) Absolute configurations are assigned according to the Baird/Sloan modification of the Chan–Ingold–Prelag priority rules as employed by Gladysz: η^5-$C_5(CH_3)_5$ > PPh_3 > NO > COR. Stanley, K.; Baird, M. C. *J. Am. Chem. Soc.* **1975**, *97*, 6598. Sloan, T. E. *Top. Stereochem.* **1981**, *12*, 1. Constable, A. G.; Gladysz, J. A. *J. Organomet. Chem.* **1980**, *202*, C21.

Scheme IX

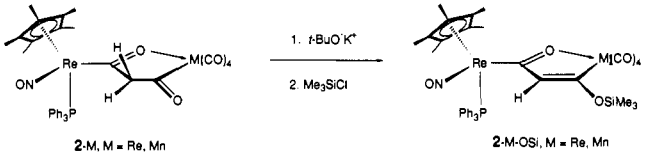

Scheme X

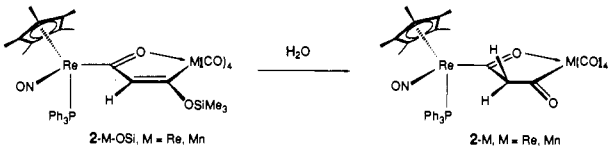

acteristic enol ligand resonances (7-Re-OH) were observed at δ 8.92 (s, 1 H) and 1.97 (s, 3 H). Integration of the respective signals led to K_{eq} = [7-OH]/[7] = 0.10 at 23 °C. In the $^{13}C\{^1H\}$ NMR spectrum of the sample, the carbonyl carbons of the malonyl ligand in 7 were observed at 299.8 (d, J = 8.4 Hz) and 268.3 ppm, whereas the corresponding resonances for 7-OH were observed at 278.1 (d, J = 9.1 Hz) and 219.3 ppm. It was possible to quantitatively generate and observe the enol complex 7-OH in THF-d_8 at −78 °C. The rhenium enolate anion was generated in situ from 2-Re and t-BuOK at −78 °C and subsequently protonated with trifluoroacetic acid at that temperature. When the sample was warmed to 15 °C, 7-OH underwent conversion to the equilibrium mixture of 7 and 7-OH, with no spectroscopic evidence for the *SS,RR* isomer 7′ (Scheme VIII).

When D_2O (175 M excess) was added to a THF-d_8 solution containing an equilibrium mixture of 7 and 7-OH, a slow incorporation of deuterium into the acidic hydrogen site of 7 was observed by ^1H NMR spectroscopy ($t_{1/2}$ > 2 weeks). There was no spectroscopic evidence for formation of the (*SS,RR*) isomer of 7 during the time required for deuterium incorporation. When deuterium incorporation was monitored by ^1H NMR spectroscopy in the presence of t-BuOK, the half-life was accelerated to 4.5 h, again with no evidence of the (*SS,RR*) diastereomer of 7. Enolization therefore occurs in 7 with no epimerization at the stereogenic carbon!

6. Trimethylsilyl Enol Ether Analogues (η^5-C_5Me_5)Re(NO)(PPh$_3$){μ-[COCH=C(OSi(CH$_3$)$_3$)}-C^1,O^3:C^3]M(CO)$_4$ (2-Re-OSi, M = Re and 2-Mn-OSi, M = Mn). In an effort to illucidate the factors responsible for the keto–enol equilibria difference between 2-Re and 2-Mn, efforts were made to isolate the corresponding enol tautomers for X-ray analysis. However, all attempts at isolation of 2-Re-OH and 2-Mn-OH met with frustration, and we therefore resorted to preparation and structural characterization of the silyl enol ether analogues, 2-Re-OSi and 2-Mn-OSi. Both analogues were prepared by deprotonation of the corresponding keto complexes and subsequent silylation with chlorotrimethylsilane (Scheme IX). In the ^1H NMR spectrum (CD_2Cl_2), the vinyl hydrogen resonance was observed at δ 6.47 for 2-Re-OSi and at 6.36 for 2-Mn-OSi. For comparison, the vinyl hydrogen resonance for 2-Re-OH was observed at δ 6.28 and for 2-Mn-OH at 6.13 (at −80 °C). In the ^{13}C NMR spectrum (CD_2Cl_2) of 2-Re-OSi, the oxygen-bearing carbons of the bridging ligand were observed at 272.6 (d, J = 11 Hz, C^3) and 223.6 (s, C^1) ppm. The corresponding signals were observed at 268.2 (d, J = 9.3 Hz) and 237.8 ppm for 2-Mn-OSi and at 270.3 (d, J = 8.5 Hz) and 224.0 for 2-Re-OH.

The observation that the keto–enol equilibrium favors the enol form for 2-Re more than for 2-Mn implies that the oxametallacyclopentene structure is less stable for manganese than rhenium, relative to the respective dicarbonyl isomers. In anticipation that this difference may also be manifested in the relative kinetic stabilities of silyl enol ethers, we measured the relative rats of hydrolysis for 2-Re-OSi and 2-Mn-OSi (Scheme X). In THF-d_8 the relative concentrations of 2-Re-OSi and 2-Mn-OSi are readily determined by integration of the vinyl hydrogen ^1H NMR resonances at δ 6.49 and 6.41, respectively. Water (35 μL, 1.93 mmol) was added to a THF-d_8 solution containing 2-Re-OSi (0.012 mmol, 35.1 mM) and 2-Mn-OSi (0.014 mmol, 39.1 mM), and the conversion to 2-M was monitored by ^1H NMR spectroscopy. In this manner, the observed rate constants for the disappearance of 2-Re-OSi and 2-Mn-OSi were determined to be 1.7 × 10^5 and 2.9 × 10^{-4} s^{-1}, respectively. Thus, the manganese complex is hydrolyzed ca. 17 times faster than the rhenium analogue.

Table II. Crystallographic Data for 2-Re-OSi and 2-Mn-OSi

	2-Re-OSi	2-Mn-OSi
	(a) Crystal Parameters	
formula	$C_{38}H_{40}NO_7PSiRe_2$	$C_{38}H_{40}NO_7PSiMnRe$
lattice type	monoclinic	monoclinic
space group	$P2_1/n$ (no. 14)	$P2_1/n$ (no. 14)
a, Å	17.741 (5)[a]	15.289 (5)
b, Å	11.745 (3)	15.278 (4)
c, Å	20.199 (7)	17.082 (4)
β, deg	108.14 (2)	93.56 (2)
V, Å^3	3999 (2)	2983 (2)
Z	4	4
cryst dimens, mm	0.42 × 0.32 × 0.38	0.46 × 0.34 × 0.41
cryst color	yellow	yellow
D(calc), g/cm^3	1.755	1.544
μ (Mo Kα), cm^{-1}	65.08	36.28
temp, °C	23	23
T(max)/T(min)	1.935	1.622
	(b) Data Collection	
radiation type	Mo Kα (λ = 0.71073 Å)	Mo Kα (λ = 0.71073 Å)
2θ range, deg	4–50	4–46
read	7198	6011
unique	6653	5540
unique obsd $F_o > 5\sigma(F_o)$	5062	3535
	(c) Refinement	
R (F) %	3.38	4.21
R (wF) %	3.60	4.25
GOF	0.996	1.068
Δ (ρ), eÅ^{-3}	1.082	0.938

[a] Unit-cell parameters from the angular settings of 25 reflections (21° ≤ 2θ ≤ 28°).

Chart II

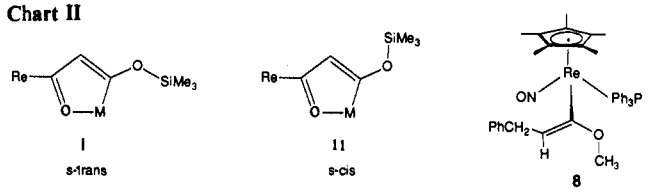

7. X-ray Structures of (η^5-C_5Me_5)Re(NO)(PPh$_3$){μ-[COCH=C(OSiMe$_3$)}-C^1,O^3:C^3]M(CO)$_4$ (2-Re-OSi, M = Re and 2-Mn-OSi, M = Mn).[16] X-ray data were acquired on a crystal of 2-Re-OSi (Figure 3) grown by cooling and slow concentration of a THF/hexanes solution (Table II). X-ray data were acquired on a crystal of 2-Mn-OSi (Figure 4) grown by cooling a toluene/hexanes solution (Table II). Selected bond distances and angles are given in Table III for both structures. The gross structural features of both complexes are qualitatively similar, with the exception of isomerism about the C(5)–OSi bond. In 2-Re-OSi the s-trans (I) silyloxy conformation is observed, whereas for 2-Mn-OSi the s-cis (II) conformation is preferred (Chart II). In most methoxyvinyl compounds the s-cis isomer is favored.[17] Gladysz recently reported the structure of an α-methoxyvinyl complex of rhenium, 8, in which the s-cis conformation was also observed (Chart II).[18,19] The s-trans conformation in 2-M-OSi

(16) X-ray structural characterization of 2-M-OSi (M = Re, Mn) was carried out at the University of Delaware.

(17) (a) Bernardi, F.; Epiotis, N. D.; Yates, R. L.; Schlegel, H. B. *J. Am. Chem. Soc.* **1976**, *98*, 2385. (b) Darig, J. R.; Compton, D. A. C. *J. Chem. Phys.* **1978**, *69*, 2028.

(18) Bodner, G. S.; Smith, D. E.; Hatton, W. G.; Heah, P. C.; Georgiou, S.; Rheingold, A. L.; Geib, S. J.; Hutchinson, J. P.; Gladysz, J. A. *J. Am. Chem. Soc.* **1987**, *109*, 7688.

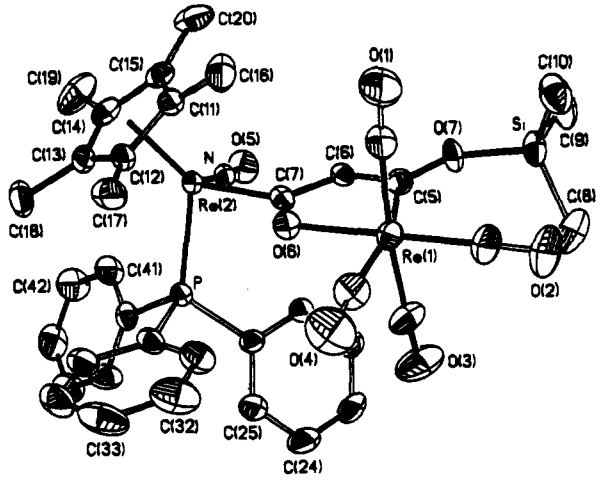

Figure 3. Structure of silyl enol ether complex $(\eta^5\text{-}C_5Me_5)(NO)(PPh_3)Re\{\mu\text{-}[COCH{=}C(OSiMe_3)]\text{-}C^1,O^3{:}C^3\}Re(CO)_4$ (**2**-Re-OSi).

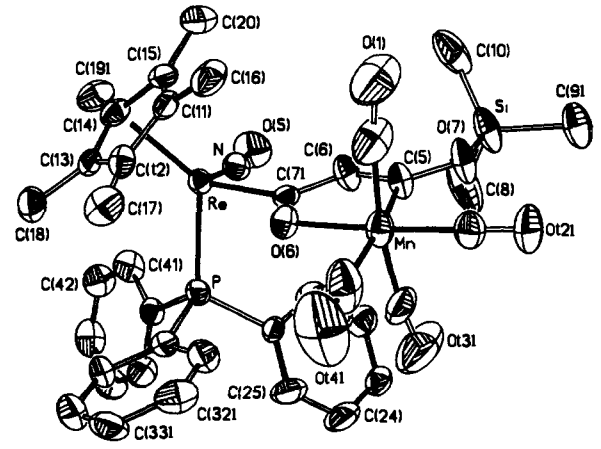

Figure 4. Structure of silyl enol ether complex $(\eta^5\text{-}C_5Me_5)(NO)(PPh_3)Re\{\mu\text{-}[COCH{=}C(OSiMe_3)]\text{-}C^1,O^3{:}C^3\}Mn(CO)_4$ (**2**-Mn-OSi).

is expected to result in an unfavorable steric interaction between the trimethylsilyl group and the C(1)–O(1) carbonyl ligand. In accordance with this view the Re(1)–C(5)–O(7) angle is 132.1 (6)°, where as the Mn–C(5)–O(7) angle is 120.7 (7)°. In the keto form of each compound the corresponding angle is ~131° (Figure 1). For comparison, the Re–C_α–O angle in **8** is 110.4 (5)°. The M–C(5)–C(6) angles in **2**-Re-OSi and **2**-Mn-OSi are constrained by the five-membered ring structure to 112.6 (6)° and 113.6 (8)°, respectively.

The ON–M–C_α–O torison angle in **2**-Re-OSi (θ = 161.8°) and **2**-Mn-OSi (θ = 168.2°) deviate significantly from the ~180° value exhibited in **2**-Re, **2**-Mn, and related malonyls and mononuclear rhenium acyls. Gladysz has also observed deviations of θ from 180° in **8** and related mononuclear complexes.[18]

8. Preparation of a Nonchelating Malonyl, $(\eta^5\text{-}C_5Me_5)(NO)(PPh_3)Re\{\mu\text{-}(COCH_2CO)\text{-}C^1{:}C^3\}Re(CO)_4(PMe_3)$ (5), from 4. In $CDCl_3$, the neutral malonyl **4** does not enolize to an observable extent. However, in THF-d_8, two very low intensity resonances were observed at δ 16.3 and 6.17 in the ^1H NMR spectrum of **4**. We attribute these signals to the enol complex **5**-OH. In an attempt to observe deuterium incorporation into the methylene hydrogens of **4**, D_2O (3 M) was added to the THF-d_8 solution. A ^1H NMR spectrum of the sample revealed the formation of a new malonyl complex (**5**) with resonances at δ 3.89 (d, J = 15.3 Hz) and 2.82 (d, J = 15.3 Hz) as well as an enol complex (**5**-OH) with a vinyl hydrogen resonance at 6.15. For comparison, in dry THF-d_8, one of the methylene hydrogens of **4** was observed at δ 4.30 (br m), and the other was obscured by the $C_5(CH_3)_5$ or PMe_3 resonances. Decomposition of these new complexes occurred over the course of 4 days with no evidence for deuterium incorporation into the methylene hydrogen sites.[20]

Scheme XI

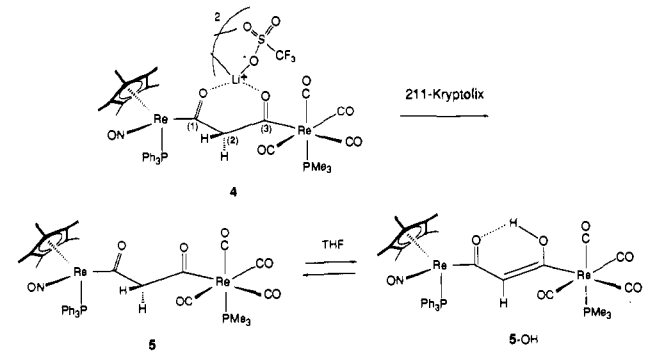

In an attempt to isolate the first example of a nonchelating μ-malonyl complex, we examined the reactivity of the lithium-chelating complex, $\{(\eta^5\text{-}C_5Me_5)(NO)(PPh_3)Re[\mu\text{-}(COCH_2CO)\text{-}C^1{:}C^3]Re(CO)_4(PMe_3)\}\cdot Li^+OSO_2CF_3^-$ (**4**), toward 211-kryptofix.[21] Addition of 211-kryptofix (0.299 mmol) to a THF (10 mL) solution of **4** (360 mg, 0.297 mmol, 30 mM) led to isolation of an orange solid (226 mg, 0.214 mmol, 72%) identified as a mixture of the nonchelating malonyl, **5**, and its enol tautomer **5**-OH (Scheme XI). In the ^1H NMR spectrum ($CDCl_3$) of the solid, resonances for **5** were observed at δ 3.94 (d, J = 15.6 Hz, 1 H), 2.73 (d, J = 15.5 Hz, 1 H), 1.70 (s, 15 H), and 1.61 (d, J = 9.3 Hz, 9 H) and resonances for **5**-OH at 16.44 (s), 6.10 (s), 1.69 (s), and 1.62 (d, J = 9.2 Hz). The low field shift of the hydroxyl proton is indicative of internal hydrogen bonding. The ratio of **5**-OH/**5** was ~0.1. In the $^{13}C\{^1H\}$ NMR spectrum ($CDCl_3$, 15 °C) two doublets at 260.4 (J = 9.1 Hz) and 250.4 (J = 10.9 Hz) are assigned to the carbonyl carbons of the malonyl ligand in **5**. Recrystallization of the orange solid from ether/hexanes at −20 °C led to a mixture of red and orange crystals which could be separated by hand. A ^1H NMR spectrum ($CDCl_3$) of the red crystals indicated a 2:9 ratio of **5**-OH to **5**, whereas the orange crystals proved to be almost entirely **5** (<0.02 ratio of **5**-OH to **5**).

In the $^{13}C\{^1H\}$ NMR spectrum of a THF-d_8 solution containing **5**-OH and **5** (0.3:1.0 ratio), one of the carbons (C^1 or C^3) of the bridging ligand in **5**-OH was observed at 249.3 ppm (d, J = 9.2 Hz). The other carbon (C^1 or C^3) resonance could not be unambiguously distinguished from the carbonyl carbon resonances; however, it is undoubtedly either a signal at 195.1 (dd, J = 12.6, 5.0 Hz) or one of the carbon resonances between 195 and 189 ppm. From the chemical shift data and X-ray analysis (vide infra) we propose a structure for **5**-OH in which the double bond is largely localized on the side of the rhenium carbonyl center (Scheme XI).

The keto–enol equilibrium at 23 °C was approached from both directions (**5** → **5**-OH and **5**-OH → **5**) by allowing a THF-d_8 solution of the red crystals and a THF-d_8 solution of the orange crystals to each equilibrate over the course of 1 week; $K_{eq}^{23°C}$ = [**5**-OH]/[**5**] = 0.65.

As anticipated, attempts to determine the degree of stereoselectivity in the enolization of **5** (32.2 mM) in the presence of D_2O (3 M) were thwarted by the decomposition of **5**, which occurred at a faster rate than that of deuterium incorporation into the methylene hydrogen sites. The diastereotopic methylene resonances at δ 2.87 and 3.84 in the ^1H NMR spectrum of **5** were monitored over the first 2 half-lives (22 h) of decomposition. The d_1 isomers would have been observed as broad resonances 0.01–0.05 ppm upfield of methylene hydrogen resonances, as was the case for **2**-Re and **2**-Mn. Ketonization of **5**-OH is clearly very slow under these conditions, as the concentration of **5**-OH in the sample (~1 mM) remained constant over the course of 6 days,

(19) For a structurally characterized (trimethylsiloxy)buta-1,3-diene, see: Gupta, R. C.; Larsen, D. S.; Stoodley, R. J.; Slawin, A. M. Z.; Williams, D. J. *J. Chem. Soc., Perkin Trans. 1* **1989**, 739.

(20) By NMR spectroscopy, the decomposition of **5** appeared to give a mixture of products which results from fragmentation of the malonyl ligand.

(21) 4,7,13,18-Tetraoxa-1,10-diazabicyclo[8.8.8]eicosane.

Table III. Selected Bond Distances and Angles for 2-Re-OSi and 2-Mn-OSi

	2-Re-OSi	2-Mn-OSi		2-Re-OSi	2-Mn-OSi
		(a) Bond Distances (Å)			
Re(2)[Re][a]-CNT[b]	1.980 (7)	1.983 (9)	Re(1)[Mn]-C(5)	2.191 (9)	1.997 (11)
Re(2)[Re]-P	2.388 (2)	2.379 (3)	Re(1)[Mn]-O(6)	2.161 (5)	2.043 (6)
Re(2)[Re]-N	1.740 (7)	1.749 (9)	C(5)-O(7)	1.358 (10)	1.363 (13)
Re(2)[Re]-C(7)	2.082 (7)	2.086 (9)	O(7)-Si	1.666 (6)	1.678 (9)
Re(1)[Mn]-C(1)	2.012 (8)	1.786 (17)	C(5)-C(6)	1.356 (10)	1.359 (14)
Re(1)[Mn]-C(2)	1.917 (9)	1.797 (12)	C(6)-C(7)	1.434 (10)	1.395 (15)
Re(1)[Mn]-C(3)	1.992 (9)	1.858 (16)	C(7)-O(6)	1.294 (10)	1.274 (11)
Re(1)[Mn]-C(4)	1.957 (11)	1.807 (17)			
		(b) Bond Angles			
CNT-Re(2)[Re]-P	126.5 (2)	129.1 (3)	C(3)-Re(1)[Mn]-C(4)	92.2 (4)	89.9 (7)
CNT-Re(2)[Re]-N	126.3 (2)	122.7 (3)	C(3)-Re(1)[Mn]-C(5)	86.4 (4)	83.9 (6)
CNT-Re(2)[Re]-C(7)	116.6 (2)	117.5 (3)	C(3)-Re(1)[Mn]-O(6)	93.1 (3)	91.4 (5)
P-Re(2)[Re]-N	93.6 (2)	93.4 (3)	C(4)-Re(1)[Mn]-C(5)	164.4 (3)	167.1 (6)
P-Re(2)[Re]-C(7)	88.4 (2)	87.8 (3)	C(4)-Re(1)[Mn]-O(6)	89.4 (3)	90.5 (5)
N-Re(2)[Re]-C(7)	95.9 (3)	97.5 (4)	C(5)-Re(1)[Mn]-O(6)	75.2 (2)	78.4 (4)
C(1)-Re(1)[Mn]-C(2)	88.2 (3)	86.3 (6)	Re(2)[Re]-C(7)-O(6)	120.3 (5)	120.2 (7)
C(1)-Re(1)[Mn]-C(3)	173.6 (4)	167.3 (8)	Re(2)[Re]-C(7)-C(6)	123.0 (6)	123.4 (7)
C(1)-Re(1)[Mn]-C(4)	92.5 (4)	102.4 (8)	Re(1)[Mn]-O(6)-C(7)	117.2 (4)	115.7 (6)
C(1)-Re(1)[Mn]-C(5)	90.3 (3)	84.7 (6)	O(6)-C(7)-C(6)	116.3 (6)	115.8 (8)
C(1)-Re(1)[Mn]-O(6)	91.3 (3)	91.7 (5)	C(7)-C(6)-C(5)	118.5 (7)	116.4 (9)
C(2)-Re(1)[Mn]-C(3)	87.4 (4)	89.7 (6)	C(6)-C(5)-Re(1)[Mn]	112.6 (6)	113.6 (8)
C(2)-Re(1)[Mn]-C(4)	90.3 (4)	93.5 (6)	C(6)-C(5)-O(7)	115.3 (8)	125.7 (9)
C(2)-Re(1)[Mn]-C(5)	105.1 (4)	97.7 (5)	Re(1)[Mn]-C(5)-O(7)	132.1 (6)	120.7 (7)
C(2)-Re(1)[Mn]-C(6)	179.5 (3)	175.8 (5)	C(5)-O(7)-Si	134.8 (6)	128.1 (6)

[a] Atom in brackets refers to 2-Mn-OSi. [b] CNT = Cp ring centroid.

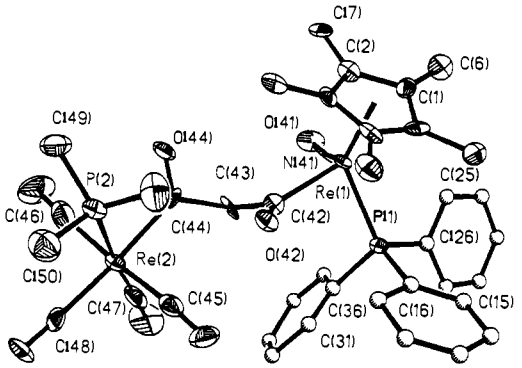

Figure 5. Structure of the nonchelating malonyl $\{(\eta^5\text{-}C_5Me_5)(NO)(PPh_3)Re[\mu\text{-}COCH_2CO)\text{-}C^1{:}C^3]Re(CO)_4(PMe_3)\}$ (**5**).

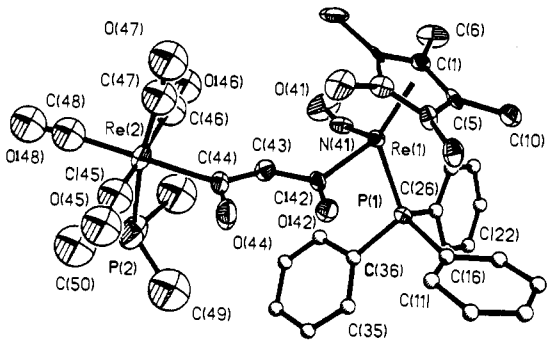

Figure 6. Structure of the enol complex, $\{(\eta^5\text{-}C_5Me_5)(NO)(PPh_3)Re[\mu\text{-}(COCHCOH)\text{-}C^1{:}C^3]Re(CO)_4(PMe_3)\}$ (**5-OH**).

even after decomposition of **5** was complete.

9. X-ray Structures of $(\eta^5\text{-}C_5Me_5)(NO)(PPh_3)Re[\mu\text{-}(COCH_2CO)\text{-}C^1{:}C^3]Re(CO)_4(PMe_3)$ (5) and $(\eta^5\text{-}C_5Me_5)(NO)(PPh_3)Re[\mu\text{-}[COCH{=}C(OH)]\text{-}C^1{:}C^3]Re(CO)_4(PMe_3)$ (5-OH).[22] X-ray data were acquired on crystals of **5** (Figure 5) and **5-OH** (Figure 6) which were cocrystallized from diffusion of hexanes into a toluene solution (Table IV). Selected bond distances and angles are given in Table V for both structures. Isomer **5** crystallized in thin plates which resulted in uncompensated absorption; however, the structure is of sufficient quality to comment on certain bond distances, geometry, and malonyl ligand conformation. It is clear that the presence of hydrogen bonding in **5-OH** and lithium ion chelation in **4** (Figure 7) dramatically effects the malonyl ligand conformation. The torsion angles for the malonyl ligand in **4**, **5**, and **5-OH** are given in Table VI. The most striking feature in **5** is the severe twist of the C(44)–O(44) carbonyl out of the Re(1), C(42), O(42) plane, which places the two malonyl oxygens at a 3.38-Å nonbonded distance. For comparison, the

(22) X-ray structural characterization of **5** and **5-OH** was carried out at the University of Wyoming.

Table IV. Crystallographic Data for **5** and **5-OH**

	5	5-OH
	(a) Crystal Parameters	
formula	$C_{38}H_{41}NO_7P_2Re_2$	$C_{38}H_{41}NO_7P_2Re_2$
lattice type	triclinic	monoclinic
space group	$P\bar{1}$	$P2_1/c$
a, Å	8.912 (5)	25.163 (4)
b, Å	11.277 (5)	9.631 (10)
c, Å	23.282 (13)	16.605 (4)
α, deg	78.54 (4)	
β, deg	89.63 (4)	96.76 (2)
γ, deg	67.99 (4)	
V, Å^3	2120 (2)	3996.2 (12)
Z	2	4
cryst dimens, mm	0.05 × 0.20 × 0.80	0.12 × 0.14 × 0.45
cryst color	yellow	orange
D (calc), g/cm^3	1.657 Mg/m^3	1.759 Mg/m^3
μ (Mo Kα), cm^{-1}	5.90	6.26
temp, °C	20	20
T(max)/T(min)	0.0469/0.1386	0.039/0.050
	(b) Data Collection	
radiation type	Mo Kα (λ = 0.71073 Å)	Mo Kα (λ = 0.71073 Å)
2θ range, deg	4.0–42.0	4.0–45.0
read	4935	5868
unique	4559	5258
unique obsd $F_o > 6\sigma(F_o)$	2925	2453
	(c) Refinement	
R (F) %	8.61	5.91
R (wF) %	10.69	7.04
GOF	1.19	1.30
Δ (ρ), eÅ^{-3}	0.058, 0.003	0.060, 0.003

Scheme XII

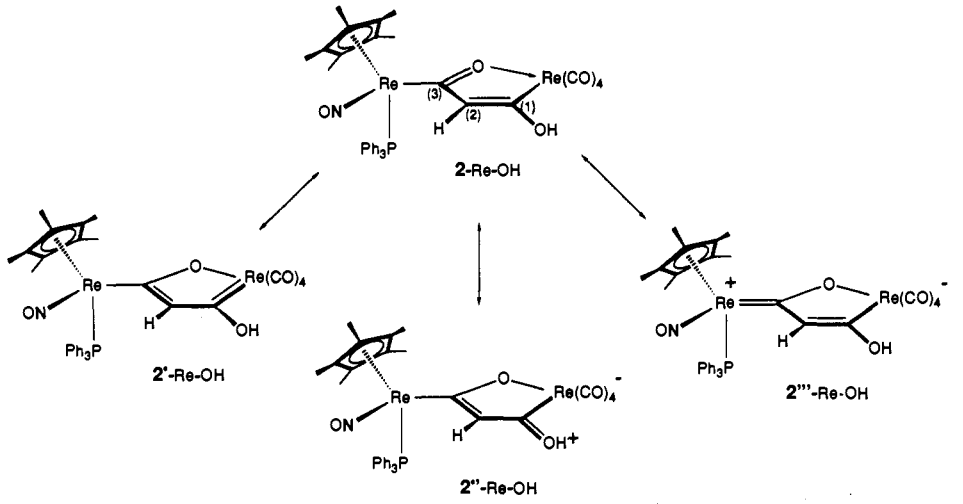

Table V. Selected Bond Distances and Angles for **4**, **5**, and **5-OH**

(a) Bond Distances (Å)

A	B	4	5	5-OH
Re(1)	P(1)	2.386 (3)	2.376 (8)	2.341 (6)
Re(1)	C(42)	2.069 (9)	2.110 (37)	2.141 (27)
Re(1)	N(41)	1.760 (9)	1.707 (25)	1.769 (23)
Re(2)	P(2)	2.453 (5)	2.473 (12)	2.369 (14)
Re(2)	C(44)	2.194 (11)	2.169 (35)	2.152 (28)
N(41)	O(41)	1.200 (12)	1.226 (33)	1.212 (33)
C(42)	O(42)	1.228 (12)	1.281 (39)	1.251 (34)
C(42)	C(43)	1.563 (16)	1.460 (45)	1.458 (37)
C(43)	C(44)	1.516 (16)	1.608 (57)	1.417 (41)
C(44)	O(44)	1.254 (13)	1.201 (35)	1.403 (42)

(b) Bond Angles (deg)

A	B	C	4	5	5-OH
P(1)	Re(1)	N(41)	91.4 (3)	92.8 (10)	92.8 (7)
P(1)	Re(1)	C(42)	86.6 (3)	85.9 (9)	86.9 (7)
N(41)	Re(1)	C(42)	97.2 (4)	95.3 (12)	98.3 (10)
P(2)	Re(2)	C(44)	84.3 (3)	82.5 (11)	88.8 (9)
Re(1)	N(41)	O(41)	172.3 (9)	171.3 (24)	165.5 (20)
Re(1)	(42)	C(43)	120.5 (7)	121.3 (22)	115.2 (19)
Re(1)	C(42)	O(42)	124.9 (8)	119.7 (23)	122.5 (19)
O(42)	C(42)	C(43)	114.6 (8)	118.0 (32)	121.9 (24)
C(42)	C(43)	C(44)	116.5 (9)	109.8 (31)	119.4 (25)
Re(2)	C(44)	C(43)	123.6 (7)	123.9 (20)	125.2 (23)
Re(2)	C(44)	O(44)	119.9 (8)	126.0 (28)	116.4 (20)
C(43)	C(44)	O(44)	116.4 (9)	107.8 (29)	118.4 (24)

Table VI. Torsion Angles (deg) for **4**, **5**, and **5-OH**

	4	5	5-OH
O(42)–C(42)–C(43)–C(44)	52.9	32.7	12.7
C(42)–C(43)–C(44)–O(44)	-51.6	90.7	-9.4
P(2)–Re(2)–C(44)–O(44)	-77.1	-56.6	-91.4
N(41)–Re(1)–C(42)–O(42)	178.5	-176.8	165.6
P(1)–Re(1)–C(42)–O(42)	90.6	90.8	73.1
O(44)–C(44)–C(42)–O(42)		109.2	2.5
P(2)–Re(2)–Re(1)–P(1)		133.7	-15.2

lithium-chelating complex **4** has an oxygen–oxygen distance of 2.80 Å, and enol complex **5-OH** exhibits a 2.50-Å oxygen–oxygen distance. The C(42)–C(43)–C(44)–O(44) torsion angle is 91° for **5**, -9.6° for **5-OH**, and -51.6° for **4**. The lithium-chelating malonyl ligand in **4** is puckered at C(43) such that the hydrogen atoms on C(43) occupy pseudoaxial and pseudoequatorial positions. The six-membered ring containing lithium adopts a boat conformation. The mean planes for the malonyl atoms C(42), C(43), C(44), O(42), and O(44) are given in Table VII. The malonyl ligand in **5-OH** exhibits only minor deviations from planarity, as expected for a hydroxypropenone structure, with largest deviation at C(42), -0.05 Å. For comparison, in the nonplanar malonyl ligand of **5**, the largest deviations are at C(42), -0.35 Å, and O(44), -0.45 Å. In both **4** and **5-OH** the two phosphine ligands are located on the same side of the chelate ring. The P(2)–Re(2)–Re(1)–P(1) torsion angle is 133.7° in **5** and -15.2° in **5-OH**. Removal of the lithium ion from **4** has resulted in a rotation about the C(43)–C(44) and Re(2)–C(44) bonds such that the $P(CH_3)_3$ ligand is positioned away from the PPh_3 ligand. The enol ligand of **5-OH** exists as a localized structure with C(42)–O(42) [1.251 (34) Å] significantly shorter than C(44)–O(44) [1.403 (42) Å]. In **4** the corresponding bond lengths are 1.228 (12) and 1.254 (13) Å, respectively. The C(42)–C(43) and C(43)–C(44) distances are not distinguishable within the error limits. The localized structure is consistent with the ^{13}C NMR data for which C(42)/C(44) are observed at 249.3 and 195 ppm. Although the NMR data does not allow determination of which localized structure is favored, the X-ray data support a C(44)–C(43) double bond.

Table VII. Least-Squares Planes for Bridging Ligands in **4**, **5**, and **5-OH**

	4	5	5-OH
C(42)	-0.2024	-0.3505	-0.0531
C(43)	0.2498	0.1474	0.0519
C(44)	-0.1877	0.5240	-0.0292
O(42)	0.0794	0.1306	0.0270
O(44)	0.0608	-0.4514	0.0035

Discussion

1. Keto–Enol Tautomerization in 2-Re, 2-Mn, and 7. The enolization chemistry described herein constitutes the first direct observation of metal–enol complexes under conditions of equilibrium with an acyl tautomer. Of the six μ-malonyl complexes studied (**2-Re**, **2-Mn**, **3**, **4**, **5**, and **7**) only **2-Mn** and the anionic lithium-chelating malonyl **3** failed to give observable amounts of an enol isomer. The existence of **2-Re-OH** in equilibrium with **2-Re** in THF-d_8 is indicated by the observation of a vinyl hydrogen resonance at δ 6.28 and a downfield hydroxyl hydrogen singlet at 8.91 in the ^1H NMR spectrum (Table I). In the $^{13}C\{^1H\}$ NMR spectrum of **2-Re-OH**, the hydroxy carbon (C^1) chemical shift is observed at 224 ppm, a 50-ppm upfield shift from the analogous carbon (C^3) in **2-Re**. In contrast, C^3 in **2-Re-OH** (270 ppm) is shifted upfield only 20 ppm from the analogous carbon resonance in **2-Re** (290 ppm). These chemical shift values indicate a large increase in electron density at C^1 and a smaller increase in electron density at C^3 in **2-Re-OSi**, as compared to **2-Re**. The observed chemical shifts (and structural data, vide infra) are consistent with the resonance structures shown in Scheme XII. The major contributors appear to be **2-Re-OH** and **2'''-Re-OH** in which C^3 has a greater degree of acyl/carbene character than C^1. Structure **2'-Re-OH** and **2''-Re-OH** account for the observation that C^1 is somewhat downfield of the expected value for a hydroxy vinyl carbon resonance.[18]

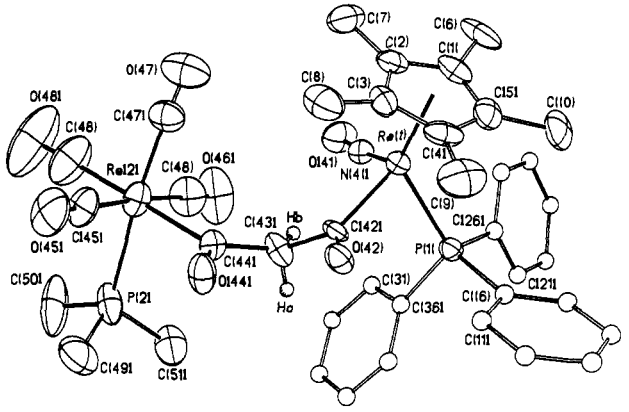

Figure 7. Structure of the lithium-chelating malonyl $\{(\eta^5\text{-}C_5Me_5)(NO)(PPh_3)Re[\mu\text{-}(COCH_2CO)\text{-}C^1{:}C^3]Re(CO)_4(PMe_3)\}\cdot Li^+OSO_2CF_3^-$ (**4**) with $LiOSO_2CF_3$ omitted.

Enolization of **2**-Re was determined to be a kinetic stereoselective process based on ^1H NMR studies which indicate differential rates of deuterium exchange from D_2O into the malonyl hydrogen sites. Incorporation of deuterium into **2**-Re and **2**-Re-OH occurs on three distinct time scales. The hydroxyl hydrogen immediately exchanges with D_2O to give **2**-Re-OD. The exo hydrogen of **2**-Re then incorporates deuterium at a slower rate ($t_{1/2} \approx 3.5$ min) to give **2**-Re-d_1. Finally, after >95% conversion to **2**-Re-d_1 and **2**-Re-OD, deuterium is incorporated into the vinyl hydrogen and endo hydrogen sites ($t_{1/2} \approx 117$ min) to give **2**-Re-d_2 and **2**-Re-d-OD (Scheme II). In a separate experiment, which employed higher concentrations of D_2O and metal complex, $t_{1/2} = 10$ and 216 min for exo and endo hydrogen exchange, respectively. The range of values for $t_{1/2}$ in these separate experiments probably indicates the presence of adventitious acid or base or solvent effects. Despite the range in rates, exo hydrogen in **2**-Re undergoes enolization 20–30 times faster than the endo hydrogen. This kinetic stereoselectivity is readily understood by examination of the solid-state structure of **2**-Re (Figure 1). The combination of the stereogenic rhenium center and the favored 180° ON–Re–C_α–O torsion angle situates the bulky PPh_3 ligand to one side of the oxametallacycle plane. The $C_5(CH_3)_5$ ligand is located on the opposite side of the metallacycle ligand but is bent back away from the methylene hydrogens. The net effect is a large difference in the accessibility of the endo and exo hydrogens to external reagents. These features have been illucidated and described in detail by Gladysz for mononuclear rhenium systems.[5u,7,13] Discrimination between the two faces of the oxametallacycle is also responsible for the stereoselective alkylation of **2**-Re to give **7**. An additional, presumably minor, factor which may impinge on the relative rates of exo and endo hydrogen enolization is a stereoelectronic effect. In the solid-state structure of **2**-Re the methylene carbon of the chelate ring is slightly puckered up away from the PPh_3 ligand. This conformation places the exo hydrogen in a pseudoaxial position and the endo hydrogen in a pseudoequatorial position. Thus, stereoelectronic effects would also favor more rapid enolization of the exo hydrogen. Both steric and stereoelectronic effects operate in the same direction.

In the case of methyl-substituted malonyl **7**, the enol complex **7**-OH is also observed spectroscopically. For **2**-Re, K_{eq} = [**2**-Re-OH]/[**2**-Re] ≈ 0.66 in THF in 23 °C, whereas for **7**, K_{eq} = [**7**-OH]/[**7**] ≈ 0.1. In organic enols, substitution of a methyl group at the β-carbon shifts the equilibrium toward the enol form by stabilization of the alkene.[23] In the case of **7** the equilibrium is shifted toward the keto form. This may be the result of steric congestion between the methyl substituent and the nitrosyl ligand in **7**-OH, assuming a ON–Re–C_α–O torsion angle of 160–180°, as was observed in the solid-state structures of **2**-M-OSi and **5**-OH. The relatively slow rate of deuterium incorporation into the acidic site of **7** is undoubtedly related to steric congestion.

In contrast to **2**-Re and **7**, the manganese complex **2**-Mn does not give observable amounts of the enol form in THF, by ^1H NMR spectroscopy. However, in the presence of D_2O, **2**-Mn does undergo stereoselective incorporation of deuterium into the methylene hydrogen sites. The exo hydrogen undergoes exchange 11 times faster than the endo hydrogen. The implication is that **2**-Mn is in equilibrium with **2**-Mn-OH but that the equilibrium lies far to the keto side. It was possible to generate the manganese enol tautomer directly by kinetic protonation of the enolate oxygen of **2**-Mn-OLi at −80 °C. Upon warming the sample to room temperature, **2**-Mn-OH was completely converted to **2**-Mn, as determined by ^1H NMR spectroscopy. Assuming that the enol complex does in fact exist in equilibrium with the keto form, then K_{eq} = [**2**-Mn-OH]/[**2**-Mn] < 0.02. In order to directly compare the relative rates of enolization in **2**-Re and **2**-Mn, D_2O was added to a THF solution containing both compounds. By ^1H NMR spectroscopic analysis, the exo hydrogen of **2**-Re was determined to undergo exchange with deuterium ten times faster, and the endo hydrogen six times faster, than for **2**-Mn.

2. Synthesis and Characterization of 2-Re-OSi and 2-Mn-OSi. In an effort to illucidate the structural factors which may influence the keto–enol equilibria in **2**-M (M = Re, Mn), we prepared and structurally characterized the trimethylsiloxy enol ether derivatives **2**-M-OSi (M = Re, Mn). The stabilities of **2**-M-OSi toward water follow the same pattern as that observed for the enolization behavior of **2**-M; that is, the manganese analogue hydrolyzes ca. 17 times faster than the rhenium analogue. Again, the implication is that the oxametallacyclopentene structure is less stable for manganese than rhenium, relative to the diacyl structure.

In an attempt to identify the structural features which may be responsible for the observed differences in the chemistry of the manganese and rhenium systems, we structurally characterized **2**-Mn-OSi and **2**-Re-OSi, for comparison with the structures of **2**-Mn and **2**-Re (Chart III). Related oxametallacycles of manganese (**9**)[24] and rhenium (**10**)[25] are included in Chart III for comparison with **2**-M-OSi. As anticipated, in **2**-Re-OSi the Re(1)–C(5) and Re(1)–O(6) distances of 2.191 (6) and 2.161 (9) Å, respectively, are longer than the corresponding Mn–C(5) and Mn–O(6) distances of 1.997 (11) and 2.043 (6) Å. The remaining distances within the bridging ligand are remarkably similar for the two complexes. In particular, there appears to be little difference in malonyl ligand bonding to the $(\eta^5\text{-}C_5Me_5)(NO)(PPh_3)$Re– center in the two complexes. The Re(2)–C(7) distances of 2.082 (7) and 2.086 (9) Å for **2**-Re-OSi and **2**-Mn-OSi, respectively, are nearly identical and indicate a significant degree of metal–carbon double bond character (although not as great as in **2**-M), as shown in resonance structure **2'''**-M-OSi (Scheme XII). In addition, the C(5)–C(6) distances of 1.356 (10) and 1.359 (14) Å for **2**-Re-OSi and **2**-Mn-OSi are within the expected range for a carbon–carbon double bond, and the C(6)–C(7) distances of 1.434 (10) and 1.395 (15) Å are significantly shorter than the sp^2–sp^2 single bond length of 1.48 in butadiene. These latter bond distances are consistent with the delocalized metallafuran resonance contribution shown for **2'**-M-OSi in Scheme XII.

The difference in the keto–enol equilibrium constants in the rhenium and manganese systems could possibly be ascribed to more aromatic stabilization in **2**-Re-OH than in **2**-Mn-OH.[24] The key structural parameter in determining whether the metallafuran rings are significantly aromatic is the metal–oxygen bond distance. In comparing the solid-state structures of the keto (**2**-M) and enol (**2**-M-OSi) complexes, it is clear that the metal–oxygen distance remains unchanged in each set: **2**-Mn [2.164 (3)], **2**-Mn-OSi [2.043 (6)] and **2**-Re [2.164(3)], **2**-Re-OSi [2.161 (9)]. Thus we conclude that aromaticity is not responsible for the observed

(23) Hine, J. *Structural Effects on Equilibria in Organic Chemistry*; Wiley-Interscience: New York, 1975; pp 270–276.

(24) DeShong, P.; Slough, G. A.; Sidler, D. R.; Rybczynski, P. J.; Von Philipsborn, W.; Kunz, R. W.; Bursten, B. E.; Clayton, T. W., Jr. *Organometallics* **1989**, *8*, 1381.

(25) Stack, J. G.; Simpson, R. D.; Hollander, F. J.; Bergman, R. G.; Heathcock, C. H. *J. Am. Chem. Soc.* **1990**, *112*, 2716.

Chart III

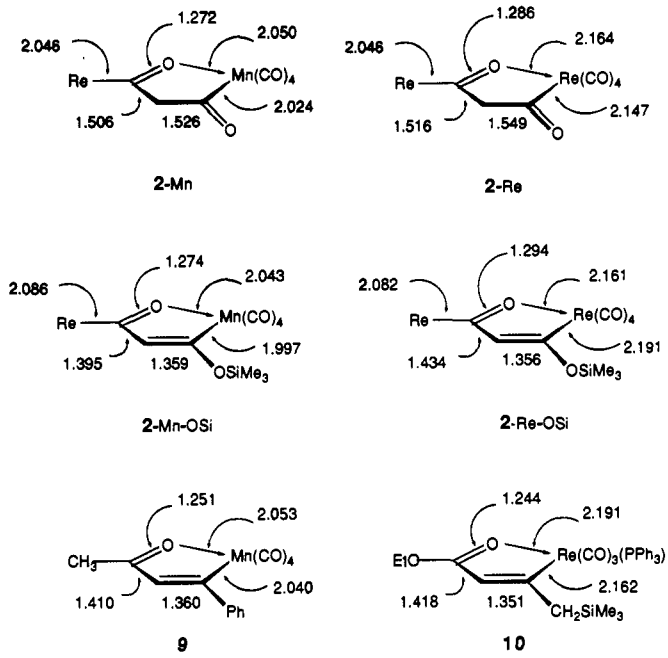

differences in the keto–enol equilibrium constants for **2**-Re and **2**-Mn.

3. Acidity of 2-M. Keto–enol tautomerization was not previously observed in metal–acyl complexes because of the weak acidity at the α-carbon. In most metal–acyl complexes the metal donates approximately the same amount of electron density into the carbonyl as an $-NR_2$ substituent in amides.[26] In the malonyl complexes reported herein, the α-hydrogens are expected to be activated relative to those of simple metal acyls, due to the acidifying effect of two carbonyl groups. In **2**-M, one of the carbonyls is further activated by oxygen coordination to one of the transition metals. In an effort to quantitate the acidity in **2**-M, we carried out a series of competition experiments with common acids. In THF solution, **2**-Re-OLi is 59% protonated upon addition of dimethyl malonate (1 equiv). Under similar conditions an equivalent of methanol fails to protonate **2**-Re-OLi, and an equivalent of methyl acetoacetate completely protonates **2**-Re-OLi. Thus it appears that the two metal centers in **2**-Re have an effect on methylene hydrogen acidity which is comparable to the two methoxy groups in dimethyl malonate. A competition experiment between **2**-Re-OLi and **2**-Mn confirmed that **2**-Re is more acidic than **2**-Mn; with the microscopic acidity K = [**2**-Re-OLi][**2**-Mn]/[**2**-Re][**2**-Mn-OLi] = 80 at −80 °C.

The observed differences in K_{eq} for enolization of **2**-Re and **2**-Mn are clearly related to destabilization of the oxametallacyclopentene structure in the manganese case relative to rhenium. On the basis of structural studies on **2**-Re, **2**-Mn, **2**-Re-OSi, and **2**-Mn-OSi, we conclude that there are no unambiguous steric or strain factors which readily account for the observed differences.

In organic systems conjugation of enols with carbon–carbon double bonds stabilizes the enol tautomer,[27] as does increased electron withdrawal by the α-substituents.[2c] The former effect is related to the rhenium-C^3 double bond character in **2**-M-OSi, which is essentially identical for both **2**-Mn-OSi and **2**-Re-OSi based on the bond distances. The question of electron withdrawal by the α-substituents is related to the difficult question of electronegativity at the manganese and rhenium carbonyl units. The hydroxy carbon resonance in the ^{13}C NMR spectra is at 238 ppm for **2**-Mn-OSi and at 224 for **2**-Re-OSi. This chemical shift difference may indicate that the rhenium carbonyl fragment donates more electron density into C^1 than does the manganese carbonyl fragment. However, we are reluctant to place undue weight on a 14-ppm chemical shift difference in the ^{13}C NMR spectra. The enolization behavior in **2**-M is complicated further by unexplained ring effects in cyclic organic ketones. For example, the enol content of cyclohexanone is greater than that of cyclopentanone or cycloheptanone.[2f]

4. Preparation of a Nonchelating μ-Malonyl Complex (5) and Structural Characterization of an Enol Complex (5-OH). The anionic malonyl **3** and the neutral malonyl **4** both exist as lithium-chelating complexes. The anionic complex is expected to bind lithium more strongly than the neutral system, and this is in accord with the observation that **3** gives rise to no observable enol complex, whereas **4** gives rise to a minor amount of the enol, **5**-OH. The observation of **5**-OH in solutions of **4** indicated that nonchelating malonyls may in fact be stable complexes. In the case of anionic malonyl **3**, lithium ion abstraction with 211-kryptofix led to rapid formation of **2**-Re, with no evidence for the enol isomer of **3**. However, it proved possible to isolate the first nonchelating μ-malonyl complex, **5**, by lithium ion abstraction from **4** with 211-kryptofix. From the spectroscopic properties of **4** and **5** it is clear that the malonyl ligand has undergone a major conformational change. In the ^1H NMR spectrum of **4**, the diastereotopic methylene hydrogens are observed at δ 1.48 (d, J = 14.6 Hz) and 5.18 (d, J = 14.7 Hz). In contrast, for **5** these resonances are observed at δ 2.73 (d, J = 15.5 Hz) and 3.94 (d, J = 15.6 Hz). The unusual chemical shift values for the methylene hydrogens in **4** are attributed to a favored malonyl ligand conformation in which one hydrogen is in the deshielding region of both carbonyl groups and the other hydrogen is shielded by a phenyl substituent on PPh_3. Removal of the lithium ion permits the molecule to adopt a less sterically demanding conformation in which the carbonyl groups no longer act in concert to deshield the methylene hydrogen. This speculation is supported by the solid-state structures of **5** (Figure 5) and **4** (Figure 7). The O(44)–C(44)–C(42)–O(42) torsion angle is 109.2° for **5** and 2.5° for the enol tautomer **5**-OH.

Initially we expected that the enol–keto equilibrium would lie further to the enol side for **5** than for **2**-Re, due to hydrogen-bonding stabilization in **5**-OH. It appears that any gain in enol stability from internal hydrogen bonding is compensated for by steric congestion between the metal coordination spheres, which forces the malonyl ligand into a nonplanar conformation. Enolization is qualitatively much slower in **5** than in **2**-M. The acidity of **5**, in the conformation shown in the solid-state structure, will be more typical of that in simple mononuclear acyls. Enolization therefore requires adaptation of a sterically less favorable conformation in which the carbonyl groups are coplanar. The net result of these steric and electronic factors is an equilibrium constant in THF (K_{eq} = [**5**-OH]/[**5**] = 0.65) that is coincidentally similar in magnitude to that observed for **2**-Re.

Conclusion

In conclusion, the first examples of keto–enol tautomerization in metal–acyl complexes have been directly observed and characterized by NMR spectroscopy. The enolization behavior varies significantly with both the conformation of the malonyl ligand and the nature of the transition metal. The observations reported here indicate that an oxametallacyclopentene structure is less stable, relative to a dicarbonyl structure, for **2**-Mn than for **2**-Re. Although the exact factors which influence this stability difference remain to be illucidated, it is clear that the stability difference does influence malonyl ligand acidity and enolization chemistry. It is now established that nonchelating complexes of the parent μ-malonyl ligand are stable, isolable species. This observation will lead to more extensive development of metal enol chemistry in the future.

Experimental Section

General Methods. All manipulations, unless otherwise stated, were performed under an atmosphere of purified nitrogen gas by using Schlenk techniques or in a Vacuum Atmospheres nitrogen box equipped with a Dri-Train MO 40-1 purifier and a −20 °F freezer. Infrared (IR) spectra were recorded on a Perkin-Elmer 1330 infrared spectrophotometer.

(26) Heah, P. C.; Patton, A. T.; Gladysz, J. A. *J. Am. Chem. Soc.* **1986**, *108*, 1185. (b) Angelici, R. J. *Acc. Chem. Res.* **1972**, *5*, 335.

(27) Capon, B.; Guo, B.-Z.; Kwok, F. C.; Siddhanta, A. K.; Zucco, C. *Acc. Chem. Res.* **1988**, *21*, 135.

Melting points were determined in sealed capillaries by using an Electrothermal melting point apparatus equipped with a calibrated thermometer. Mass spectra were performed at the University of California, Riverside Mass Spectroscopy (UCRMS) facility. Elemental analyses were performed by Galbraith Laboratories or Schwarzkopf. NMR spectra were recorded at ambient probe temperature unless otherwise stated on either a GE QE 300 (^{1}H, 300 MHz; ^{13}C, 75 MHz) or Varian UNITY 500 (^{1}H, 500 MHz; ^{13}C, 126 MHz) NMR spectrometer. ^{1}H NMR chemical shifts are reported relative to the residual protiated solvent resonance: $CDHCl_2$, δ 5.32; $CHCl_3$, 7.24; THF-d_7, 3.58. ^{13}C NMR chemical shifts are reported relative to the solvent resonance: $CDCl_3$, 77.0 ppm; CD_2Cl_2, 53.8; THF-d_8, 67.4. Dried and degassed solvents were used throughout. $ClSiMe_3$ was distilled from CaH_2 and manipulated by vacuum transfer. D_2O (Aldrich) was 99.8 atom % D. $CH_3C(O)CHCO_2CH_3Li$ was prepared from methyl acetoacetate and LDA in ether solution at −78 °C. $(CO_2Me)_2CHLi$ was prepared from $(CO_2Me)_2CH_2$ and $LiN(TMS)_2$ in ether solution at 0 °C. *t*-BuOLi was prepared from *t*-BuOH and *n*-BuLi in ether solution at 0 °C. The complexes $(\eta^5\text{-}C_5Me_5)(NO)(PPh_3)Re[\mu\text{-}(COCH_2CO)\text{-}C^1{:}C^3,O^1]Re(CO)_4$ (**2-Re**), $(\eta^5\text{-}C_5Me_5)(NO)(PPh_3)Re[\mu\text{-}(COCH_2CO)\text{-}C^1{:}C^3,O^1]Mn(CO)_4$ (**2-Mn**), and $\{(\eta^5\text{-}C_5Me_5)(NO)(PPh_3)Re[\mu\text{-}COCH_2CO)\text{-}C^1{:}C^3]Re(CO)_4(PMe_3)\}\cdot Li^+O_3SCF_3^-$ (**4**) were prepared as previously described.[6b]

Deuterium Incorporation into $(\eta^5\text{-}C_5Me_5)(NO)(PPh_3)Re[\mu\text{-}(COCH_2CO)\text{-}C^1,O^3{:}C^3]Re(CO)_4$ (2-Re). A 5-mm NMR tube was charged with **2-Re** (7.3 mg, 0.0074 mmol) and THF-d_8 (1.13 mL) was sealed with a septum under nitrogen: ^{1}H NMR for **2-Re**, δ 1.76 (s, 15 H), 2.47 (d, J = 20.5 Hz, 1 H), 3.01 (d, J = 20.5 Hz, 1 H) and for **2-Re-OH**, δ 1.73 (s, 15 H), 6.28 (s, 1 H), 8.91 (s, 1 H), 7.39 and 7.48 (br s, PPh_3). Comparison of the relative intensities of the resonances at δ 3.01 and 6.28 gave $K_{eq}^{23°C}$ = [**2-Re-OH**]/[**2-Re**] = 0.66. Deuterium oxide (47 μL, 2.08 M, 317 equiv) was added, and the disappearance of **2-Re** was monitored by ^{1}H NMR spectroscopy as the intensity decrease of the doublet at δ 3.01. The initial appearance of **2-Re-d_1** was monitored by the appearance of a new broad singlet at δ 2.44, which partially overlapped the doublet at 2.47 (**2-Re**). After 23 min, the methylene resonances for **2-Re** were absent, and the new singlet for **2-Re-d_1** had grown to 95% completion. Over the next 5 h, the new resonance for **2-Re-d_1** gradually decreased in intensity. From a plot of ln ([**2-Re**]$_0$/[**2-Re**]) vs time, the observed rate constant for the disappearance of **2-Re** was determined to be 3.4×10^{-3} s^{-1} (r = 0.99, $t_{1/2}$ = 3.4 min). In a similar fashion, the observed rate constant for the initial appearance of **2-Re-d_1** was determined to be 2.0×10^{-3} s^{-1} (r = 1.00) from a plot of ln ([**2-Re-d_1**]$_{max}$ − [**2-Re-d_1**]/[**2-Re-d_1**]$_{max}$) vs time. From a plot of ln ([**2-Re-d_1**]$_{max}$/[**2-Re-d_1**]) vs time, the observed rate constant for the final disappearance of **2-Re-d_1** was determined to be 9.9×10^{-5} s^{-1} (r = 1.00, $t_{1/2}$ = 117 min).

In a similar experiment (**2-Re**, 10.9 mg, 0.0111 mmol, 22.2 mM; THF-d_8, 0.50 mL; D_2O, 38 μL, 1.9 mmol, 3.8 M) the observed rate constant for the disappearance of **2-Re** was determined to be 1.2×10^{-3} s^{-1} (r = 0.98, $t_{1/2}$ = 9.7 m), the observed rate constant for the initial appearance of **2-Re-d_1** was determined to be 1.0×10^{-3} s^{-1} (r = −0.98, $t_{1/2}$ = 11.1 m), and the observed rate constant for the final disappearance of **2-Re-d_1** was determined to be 5.3×10^{-5} s^{-1} (r = 0.99, $t_{1/2}$ = 216 m).

Acidity of 2-Re. A 5-mm NMR tube was charged with **2-Re** (7.7 mg, 0.008 mmol, 19.6 mM), $(CO_2Me)_2CHLi$ (1.3 mg, 0.009 mmol), and THF-d_8 (0.40 mL) and then sealed under a nitrogen atmosphere. A ^{1}H NMR spectrum of the sample revealed the presence of the following compounds: $(CO_2Me)_2CHLi$ [δ 3.90 (s, 1 H), 3.41 (s, 6 H), 17.6 mM], $(CO_2Me)_2CH_2$ [δ 3.65 (s, 6 H), 3.35 (s, 2 H), 5.3 mM], **2-Re-OH** + **2-Re-OLi** [δ 6.02 (br m), 10.4 mM], **2-Re-OH** [δ 8.91 (br m), 2.0 mM], **2-Re** [δ 3.02 (d, J = 20.5 Hz), 2.49 (d, J = 20.5 Hz), 5.4 mM]. The microscopic equilibrium constant determined to be K_{eq} = [**2-Re-Li**]-[$(CO_2Me)_2CH_2$]/[**2-Re**][$(CO_2Me)_2CHLi$] = 0.5.

In a related experiment, a 5-mm NMR tube was charged with **2-Re** (16.5 mg, 0.0168 mmol, 29.5 mM), *t*-BuOLi (1.4 mg, 0.0175 mmol, 30.7 mM), and THF-d_8 (0.57 mL) and then capped with a septum under a stream of nitrogen gas. The crystalline **2-Re** was dissolved by heating the solution to reflux and by vortex mixing: ^{1}H NMR δ 1.72 (s, Cp* + THF-d_7), 5.97 (br, s, 1 H), 7.32 and 7.54 (br s, 15 H). One equivalent of *t*-BuOH was also observed at 3.19 (s, 1 H), 1.14 (s, 9 H). In the glovebox, $(CO_2Me)_2CH_2$ (1.9 μL, 0.0166 mmol, 29.1 mM) was added, and a second ^{1}H NMR spectrum was obtained: $(CO_2Me)_2CHLi$, δ 3.90 (s, 1 H), 3.41 (s, 6 H), 18.4 mM; $(CO_2Me)_2CH_2$, 3.65 (s, 6 H), 3.34 (s, 2 H), 9.0 mM; 8.90 (br s, **2-Re-OH**, 5.7 mM), 7.48 and 7.34 (br s, PPh_3), 6.07 (br s, 17.0 mM, **2-Re-OH** + **2-Re-OLi**, for **2-Re-OLi**, 11.3 mM, 3.01 (d, J = 20.4 Hz, **2-Re**, 10.5 mM), 2.49 (d, J = 20.5 Hz, **2-Re**), 1.80 (s), 1.73 (s), 3.20 (s, *t*-BuOH), 1.14 (s, *t*-BuOH). The microscopic equilibrium constant was determined to be K_{eq} = [**2-Re-Li**]-[$(CO_2Me)_2CH_2$]/[**2-Re**][$(CO_2Me)_2CHLi$] = 0.5.

Preparation of $\{(\eta^5\text{-}C_5Me_5)(NO)(PPh_3)Re[\mu\text{-}(COCH{=}CO)\text{-}C^1,O^3{:}C^3]Re(CO)_4\}^-Li^+$ (2-Re-OLi). A 5-mm NMR tube was charged with **2-Re** (39.2 mg, 0.0398 mmol, 43.8 mM), *t*-BuOLi (3.2 mg, 0.0400 mmol), and THF-d_8 (0.91 mL) and capped under a stream of nitrogen gas. The crystalline **2-Re** was dissolved by heating the solution to reflux and by vortex mixing: ^{1}H NMR δ 1.72 (s, $C_5(CH_3)_5$ + THF-d_7), 5.98 (br s, 1 H), 7.32 and 7.54 (br s, 15 H), 1.14 (s, *t*-BuOH), 3.19 (s, *t*-BuOH); ^{13}C{^{1}H} NMR (45 °C) δ 250.1 (br), 197.7 (br), 197.1 (br), 195.6 (br), 194.3 (br), 140.6 (br), 135–137 (br m), 135.3 (br m), 130.3, 128.5 (br), 102.1, 10.2. A gradual loss of lock signal was observed during the ^{13}C NMR experiment, presumably due to precipitation of an orange crystalline solid (**2-Re-OLi**), which was isolated by decanting away the solution. The solid was then placed under vacuum for 1 week: 31.3 mg; mp 252–264 °C (dec, onset of blackening ca. 210 °C): IR (KBr) 2060 (m), 1942 (s, br), 1895 (s), 1631 (m), 1478 (w), 1405 (m), 1385 (m) cm^{-1}. Anal. Calcd for $C_{35}H_{31}NO_7PRe_2\cdot$(THF-$d_8$): C, 44.19; H, 3.71. Found: C, 44.24; H, 4.00.

Protonation of 2-Re-Li. A 5-mm NMR tube was charged with **2-Re** (27.4 mg, 0.0279 mmol, 46 mM), *t*-BuOLi (2.3 mg, 0.0288 mmol, 48 mM), and THF-d_8 (0.6 mL) and capped with a septum under a stream of nitrogen gas. The crystalline **2-Re** was dissolved by heating the solution to reflux with a heat gun and by vortex mixing: ^{1}H NMR δ 7.52 and 7.32 (br s, PPh_3), 6.22 (br s, 1 H), 1.72 (s, Cp* + THF), 3.21 (s, *t*-BuOH), 1.14 (s, *t*-BuOH). The tube was placed in a −78 °C bath, and an orange solid precipitated. CF_3CO_2H (2.2 μL, 0.0286 mmol, 48 mM) was added, and the tube was placed on a vortex mixer for brief intervals while attempting to maintain the tube at −78 °C. A white solid was allowed to settle from the yellow solution before the tube was placed into a precooled NMR probe: ^{1}H NMR (−80 °C) δ 9.43 (s, **2-Re-OH**), 6.22 (s, **2-Re-OH**), 3.08 (d, J = 20.7 Hz, **2-Re**), 2.14 (d, J = 20.7 Hz, **2-Re**); [**2-Re-OLi**]/[**2-Re**] = 2.3 (only products observed); ^{13}C{^{1}H} NMR (−80 °C), for **2-Re-OH** δ 270.3 (d, J = 8.5 Hz, $PPh_3ReCOCH_2$), 224.0 ($ReCOCH_2$), 194.7 (ReCO), 193.3 (ReCO), 191.3 (ReCO), 189.6 (ReCO), 139.8–128.7 (m, C_6H_5 for both **2-Re-OH** and **2-Re**), 103.2 (C_5Me_5), 10.1 (C_5Me_5); for **2-Re** δ 291.4 (d, J = 8.5 Hz, $PPh_3ReCOCH_2$), 267.8 ($ReCOCH_2$), 196.5 (ReCO), 193.4 (ReCO), 193.1 (ReCO) (only three ReCO resonances were observed), 104.4 (C_5Me_5), 95.8 ($COCH_2CO$), 9.9 (C_5Me_5); resonances for CF_3CO_2Li were observed at δ 161.1 (q, J = 34.0 Hz), 118.0 (q, J = 293 Hz). After 9 h at −80 °C, [**2-Re-OH**]/[**2-Re**] = 2.2.

Deuterium Incorporation into $(\eta^5\text{-}C_5Me_5)(NO)(PPh_3)Re[\mu\text{-}(COCH_2CO)\text{-}C^1,O^3{:}C^3]Mn(CO)_4$ (2-Mn). A 5-mm NMR tube was charged with **2-Mn** (11.0 mg, 0.013 mmol) and THF-d_8 (0.60 mL), and the tube was sealed with a septum under nitrogen. An initial ^{1}H NMR spectrum indicated the presence of only **2-Mn**: δ 1.79 (s, 15 H), 2.81 (d, J = 20.0 Hz, 1 H), 3.36 (d, J = 20.0 Hz, 1 H), 7.4 (m, 15 H). Deuterium oxide (47 μL, 4.1 M) was then added. The residual HDO resonance at δ 3.38 (br) partially obscured the low field methylene hydrogen doublet of **2-Mn** at 3.36. The disappearance of **2-Mn** was monitored by the intensity decrease of the doublet at δ 2.81, and the initial appearance of **2-Mn-d_1** was monitored by the appearance of a new broad singlet at 2.77, which partially overlapped with the doublet at 2.81. After 14.3 h, the methylene resonance for **2-Mn** was absent, and a new singlet for **2-Mn-d_1** had grown to 74% completion. Over the next 4 days, the new resonance for **2-Mn-d_1** gradually decreased in intensity. From a plot of ln ([**2-Mn**]$_0$/[**2-Mn**]) vs time, the observed rate constant for disappearance of **2-Mn** was determined to be 7.8×10^{-5} s^{-1} (r = 0.99, $t_{1/2}$ = 150 min). From a plot of ln ([**2-Mn-d_1**]$_{max}$ − [**2-Mn-d_1**]/[**2-Mn-d_1**]) vs time, the observed rate constant for the initial appearance of **2-Mn-d_1** was determined to be 5.8×10^{-5} s^{-1} (r = 0.99). From a plot of ln ([**2-Mn-d_1**]$_{max}$/[**2-Mn-d_1**] vs time, the observed rate constant for the final disappearance of **2-Mn-d_1** was determined to be 5.3×10^{-6} s^{-1} (r = 0.99, $t_{1/2}$ = 36 h).

Generation and Protonation of $\{(\eta^5\text{-}C_5Me_5)(NO)(PPh_3)Re[\mu\text{-}(COCH{=}CO)\text{-}C^1,O^3{:}C^3]Mn(CO)_4\}^-Li^+$ (2-MnOLi). A 5-mm NMR tube was charged with **2-Mn** (34.9 mg, 0.0410 mmol, 44.6 mM), *t*-BuOLi (3.3 mg, 0.0413 mmol), and THF-d_8 (0.92 mL) and then capped under a stream of nitrogen gas: ^{1}H NMR δ 1.69 (s, 15 H), 5.79 (br s, $\nu_{1/2}$ = 40 Hz, 1 H), 7.30 and 7.52 (br s, 15 H), 1.14 (s, *t*-BuOH, 9 H), 3.20 (s, *t*-BuOH, 1 H). At 50 °C the singlet at 5.75 sharpened ($\nu_{1/2}$ = 18 Hz); ^{13}C{^{1}H} NMR (45 °C) δ 254.1 (br m), 246.2 (ν br m), 221.5, 219.8, 219.7, 216.0, 137–134 (br m), 135.3, 130.2, 128.4 (d, J = 8.4 Hz), 101.9, 10.2. After standing at room temperature for 2 days, a small amount of an orange solid had precipitated; however, no decomposition had occurred by ^{1}H NMR spectroscopy: ^{1}H NMR (−80 °C) δ 1.71 (s, 15 H), 5.57 (s, 0.06 H), 5.96 (s, 0.71 H), 5.99 (s, 0.24 H), 7.2–7.7 (m, 15 H), 1.15 (s, *t*-BuOH), 3.89 (s, *t*-BuOH). The sample was then placed in a −78 °C bath, CF_3CO_2H (3.2 μL, 0.0415 mmol) was added, and the NMR tube was shaken to give a homogeneous solution before returning it to the cold NMR probe: ^{1}H NMR (−80 °C) for **2-Mn**, δ 2.58 (d, J

= 21.2 Hz), 3.42 (d, J = 21.6 Hz), 25.1 mM; **2**-Mn-OH, δ 6.13 (s), 9.62 (s), 12.8 mM. After warming the probe to −25 °C, only traces of **2**-Mn-OH remained, while **2**-Mn constituted the sole product. At room temperature there was no evidence for **2**-Mn-OH.

Acidity of 2-Re vs 2-Mn. A 5-mm NMR tube was charged with **2**-Re (23.0 mg, 0.0234 mmol), *t*-BuOLi (1.9 mg, 0.0238 mmol, 45.8 mM), 1,4-$(TMS)_2C_6H_4$ as an internal standard, and THF-d_8 (0.52 mL). The tube was then closed under nitrogen gas, and a ^{1}H NMR spectrum was taken of the heterogeneous solution: ^{1}H NMR (25 °C) δ 7.34–7.52 (m, PPh_3), 5.98 (br s), 1.72 (s, Cp*), 3.19 (s, *t*-BuOH), 1.15 (s, *t*-BuOH); ^{1}H NMR (−80 °C) δ 7.2–7.7 (m, PPh_3), 6.06 (s, 0.22 H), 6.04 (s, 0.78 H), 1.69 (br s, Cp*), 3.86 (s, *t*-BuOH), 1.13 (s, *t*-BuOH). In the drybox **2**-Mn (19.6 mg, 0.0230 mmol) was added, also giving a heterogeneous solution: ^{1}H NMR (25 °C) δ 7.47 and 7.35 (br s, PPh_3, 79.7 mM), 6.00 (br s, 23.6 mM), 5.78 (br m, 5.8 mM), 3.36 (d, J = 20.6 Hz, **2**-Mn), 3.02 (d, J = 20.6 Hz, **2**-Re), 2.81 (d, J = 20.6 Hz, **2**-Mn, 28.8 mM), 2.47 (d, J = 20.6 Hz, **2**-Re, 3.1 mM), 1.80 (s), 1.78 (s), 1.72 (s), 1.70 (s); ^{1}H NMR (−80 °C), δ 7.7–7.2 (m, PPh_3, 72.7 mM), 6.22 (s, **2**-Re-OH, 1.2 mM), 6.10 (s, **2**-Mn-OH, 1.5 mM), 6.06 and 6.04 (s, 34:66, **2**-Re-OLi, 21.8 mM), 5.97 and 5.95 (s, 36:64, **2**-Mn-OLi, 5.0 mM), 3.42 (d, J = 21.0 Hz, **2**-Mn), 3.08 (d, J = 20.8 Hz, **2**-Re, 1.5 mM), 2.58 (d, J = 21.0 Hz, **2**-Mn, 27.7 mM), 2.14 (d, J = 21.2 Hz, **2**-Re), 1.78 (s), 1.69 (s), 1.67 (s); K = [**2**-Re-OLi][**2**-Mn]/[**2**-Re][**2**-Mn-OLi] = 80.

In a similar experiment, a 5-mm NMR tube was charged with **2**-Mn (8.1 mg, 0.0095 mmol, 23.8 mM), *t*-BuOLi (0.7 mg), THF-d_8 (0.40 mL), and 1,4-$(TMS)_2C_6H_4$ as an internal standard and then closed under nitrogen gas; ^{1}H NMR spectroscopy on the sample indicated the following: **2**-Mn-OLi (11.7 mM) and **2**-Mn (1.3 mM). In the glovebox, the solution was added to another 5-mm NMR tube containing **2**-Re (10.7 mg, 0.0109 mmol, 27.2 mM). The tube was closed under nitrogen gas, and the solution was briefly refluxed to dissolve the solids: ^{1}H NMR spectroscopy indicated the following: **2**-Mn (8.7 mM), **2**-Re (3.1 mM), **2**-Mn-OLi (0.8 mM). A broad singlet was observed at δ 6.02 for both **2**-Re-OH and **2**-Re-OLi (10.5 mM). At −80 °C, ^{1}H NMR spectrroscopy indicated the following: **2**-Mn (12.2 mM), **2**-Re (~2 mM), **2**-Re-OLi (9.7 mM), and **2**-Re-OH (5.0 mM). The expected resonances for **2**-Mn-OLi were very low intensity and could not be resolved from the broad multiplet observed for **2**-Re-OLi at δ 6.04.

Preparation of $(\eta^5$-$C_5Me_5)(NO)(PPh_3)Re\{\mu$-[COCH=C$(OSiMe_3)]$-$C^1,O^3$:$C^3\}Re(CO)_4$ (2-Re-OSi). A round-bottomed flask equipped with a magnetic stir bar was charged with **2**-Re (209 mg, 0.213 mmol, 14 mM), and *t*-BuOK (31 mg, 0.277 mmol). THF (15 mL) was added, and the deep orange solution was stirred until all the solids had dissolved before cooling to −78 °C. Chlorotrimethylsilane (0.5 mL, 4 mmol) was added, and the cloudy solution was allowed to warm to room temperature. The volatiles were removed under vacuum, and the residue was dissolved in CH_2Cl_2 (5 mL). Hexanes (10 mL) was added, the cloudy solution was filtered, and the solvent was removed from the filtrate under vacuum. The residue was washed with hexanes at −43 °C, to give an orange solid (**2**-Re-OSi, 191 mg, 0.181 mmol, 85%): mp 165–170°C (dec); IR (CH_2Cl_2) 2075 (m), 1966 (s), 1907 (s), 1638 (m), 1450 (m) cm^{-1}; ^{1}H NMR (CD_2Cl_2) δ 7.40 (br s, 15 H), 6.47 (s, 1 H), 1.74 (s, 15 H), 0.27 (s, 9 H); ^{13}C{^{1}H} NMR (CD_2Cl_2) δ 272.6 (d, J = 11.0 Hz, PPh_3ReCO), 223.6 ($ReCOSiMe_3$), 193.9 (ReCO), 193.9 (ReCO), 190.1 (ReCO), 189.3 (ReCO), 145.2 (COCH=C), 134.1 (C_6H_5), 130.6 (C_6H_5), 128.6 (C_6H_5), 128.5 (C_6H_5), 103.2 (C_5Me_5), 10.0 (C_5Me_5), 0.9 ($SiMe_3$); MS (FAB), m/e 1054, matched calcd isotopic distribution pattern for $C_{38}H_{40}NO_7PSiRe_2$. Anal. Calcd for $C_{38}H_{40}NO_7PSiRe_2$: C, 43.29; H, 3.82; N, 1.33. Found: C, 43.57, H, 3.79; N, 1.23.

Preparation of $(\eta^5$-$C_5Me_5)(NO)(PPh_3)Re\{\mu$-[COCH=C-$(OSiMe_3)]C^1,O^3$:$C^3\}Mn(CO)_4$ (2-Mn-OSi). A round-bottomed flask equipped with a magnetic stir bar was charged with **2**-Mn (156 mg, 0.183 mmol, 7 mM), *t*-BuOK (36 mg, 0.321 mmol), and THF (25 mL). The deep orange solution was stirred for 0.5 h and then cooled to −76 °C. Chlorotrimethylsilane (0.9 mL, 7.2 mmol) was added, and the solution was stirred at room temperature for 0.5 h. The volatiles were then removed under vacuum, and the residue was dissolved in benzene. Hexanes was added, the cloudy solution was filtered, and the solvent was removed under vacuum. The residue was taken up in benzene, hexanes was added, the solution was filtered, and the solvent was removed under vacuum to yield **2**-Mn-OSi as an orange solid (99 mg, 0.107 mmol, 59%): mp 148–152 °C (dec); IR (CH_2Cl_2) 2070 (s), 1970 (vs), 1924 (s), 1644 (s), 1460 (s), 1435 (m), 1340 (m), 1320 (m) cm^{-1}; ^{1}H NMR ($CDCl_3$) δ 7.37 (br s, 15 H), 6.36 (s, 1 H), 1.70 (s, 15 H), 0.28 (s, 9 H); ^{13}C{^{1}H} NMR ($CDCl_3$) δ 268.1 (d, J = 9.3 Hz, ReCO), 237.8 ($MnCOSiMe_3$), 218.9 (MnCO), 215.8 (MnCO), 213.5 (MnCO), 211.2 (MnCO), 138.1 (COCH=C), 133.8 (br m, C_6H_5), 130.1 (C_6H_5), 128.6 (C_6H_5), 128.2 (C_6H_5), 102.4 (C_5Me_5), 9.8 (C_5Me_5), 0.6 ($SiMe_3$). Anal. Calcd for $C_{38}H_{40}NO_7PSiMnRe$: C, 49.45; H, 4.37; N, 1.52. Found: C, 49.77; H, 4.58; N, 1.46.

Competitive Hydrolysis of 2-Re-OSi and 2-Mn-OSi. A 5-mm NMR tube was charged with **2**-Mn-OSi (12.7 mg, 0.0137 mmol, 39.1 mM), **2**-Re-OSi (13.0 mg, 0.0123 mmol, 35.1 mM), THF-d_8 (0.35 mL), and 1,4-$(TMS)_2C_6H_4$ as an internal standard. The tube was then capped with a septum under a stream of nitrogen gas, and an initial ^{1}H NMR spectrum was obtained. H_2O (35 μL, 1.93 mmol, 5.5 M) was added, and the ensuing reaction was monitored by ^{1}H NMR spectroscopy. After 4.3 h, **2**-Mn-OSi was completely consumed. The products observed were **2**-Re-OSi, 27.1 mM; **2**-Re, 4.9 mM; **2**-Re-OH, 1.9 mM; **2**-Mn, 35.7 mM. The disappearance of **2**-Mn-OSi was monitored over the first 4 h of reaction by the decrease in intensity of the singlet at δ 6.41. The disappearance of **2**-Re-OSi was monitored by the decrease in intensity of the singlet at δ 6.49. From a plot of ln ([**2**-Re-OSi]$_0$/[**2**-Re-OSi]) vs time, the observed rate constant for the disappearance of **2**-Re-OSi was determined to be 1.7×10^{-5} s^{-1} (r = 0.96), and from a plot of ln ([**2**-Mn-OSi]$_0$/[**2**-Mn-OSi]) vs time, the observed rate constant for the disappearance of **2**-Mn-OSi was determined to be 2.9×10^{-4} s^{-1} (r = 0.99, $k_{2\text{-Mn-OSi}}/k_{2\text{-Re-OSi}}$ = 17).

X-ray Crystal Structure Determinations for 2-Re-OSi and 2-Mn-OSi. In Table I crystal parameters, data collection, and refinement parameters are collected. A crystal of $C_{38}H_{40}NO_7SiRe_2$ (**2**-Re-OSi) was grown by cooling and slow concentration by evaporation of a THF/hexane solution, and a crystal of $C_{38}H_{40}NO_7SiMnRe$ (**2**-Mn-OSi) was grown by cooling a toluene/hexane solution. An empirical correction for absorption was applied to both data sets (216 ψ-scan reflections, pseudoellipsoid model). The structures of **2**-Re-OSi and **2**-Mn-OSi were solved by direct methods which located the Re atoms; the remaining non-hydrogen atoms were found by subsequent least-squares cycles and difference Fourier calculations. For both structures all non-hydrogen atoms were refined anisotropically, and hydrogens were incorporated as idealized isotropic contributions (d(CH) = 0.96 Å, U = 1.2U for attached C) and phenyl rings were fixed as rigid, planar hexagons (d(CC) = 1.395 Å). All software is contained in the SHELXTL (5.1) program library (G. Sheldrick Nicolet Corp., Madison, WI).

Atom coordinates are given in Table II for **2**-Re-OSi and Table III for **2**-Mn-OSi, and selected bond distances and angles are given in Table IV.

Preparation of $(\eta^5$-$C_5Me_5)(NO)(PPh_3)Re[\mu$-$(COCH_2CO)$-$C^1$:$C^3]$Re-$(PMe_3)(CO)_4$ (5) and $\{(\eta^5$-$C_5Me_5)(NO)(PPh_3)Re[\mu$-$(COCHCOH)$-$C^1$:$C^3]Re(CO)_4(PMe_3)\}$ (5-OH). A round-bottomed flask equipped with a magnetic stir bar was charged with **4** (360 mg, 0.297 mmol, 30 mM) and THF (10 mL). 211-Kryptofix (88 mg, 0.299 mmol) was added, and the solution was stirred for 0.5 h. The volume was then reduced under vacuum to ca. 2 mL, ether (15 mL) was added, and the solution was filtered. The solvent was removed under vacuum, and the yellow residue was dissolved in dibutyl ether. The solution was then filtered through a small plug of Celite, and the filtrates were placed in a −20 °C freezer for 4 days. An orange solid (**5** + **5**-OH) was isolated by filtration (226 mg, 0.214 mmol, 72%): mp 151–154 °C (dec); IR (CH_2Cl_2) 2085 (s), 1972 (vs, br), 1940 (s), 1632 (s), 1595 (m), 1525 (m) cm^{-1}; ^{1}H NMR ($CDCl_3$), for **5**, δ 7.38 (m, PPh_3), 3.94 (d, J = 15.6 Hz, 1 H), 2.73 (d, J = 15.5 Hz, 1 H), 1.70 (s, 15 H), 1.61 (d, J = 9.3 Hz, 9 H); for **5**-OH, 16.44 (s), 6.10 (s), 1.69 (s, Cp*), 1.62 (d, J = 9.2 Hz), [**5**-OH]/[**5**] = 0.07; ^{13}C{^{1}H} NMR ($CDCl_3$, 15 °C), for **5**, δ 260.4 (d, J = 9.1 Hz, $R_3PReCOCH_2$), 250.4 (d, J = 10.9 Hz, $R_3PReCOCH_2$), 190.3, 190.2, 190.1, 190.0, 189.1, 189.0, 188.9, 188.3 (eight lines observed for four Me_3PReCO doublets), 133.8 (br m, C_6H_5), 129.9 (C_6H_5), 128.1 (C_6H_5), 128.0 (C_6H_5), 102.5 (CH_2), 102.3 ($C_5(CH_3)_5$), 18.1 (d, J = 33.0 Hz, $P(CH_3)_3$), 9.7 ($C_5(CH_3)_5$); for **5**-OH, 140.2 (m), 129.6, 127.9, 127.8, 101.5. A THF-d_8 solution of **5** and **5**-OH was allowed to stand overnight ([**5**-OH]/[**5**] = 0.29): ^{13}C{^{1}H} NMR, for **5** δ 258.3 (d, J = 9.2 Hz, $ReCOCH_2$), 251.8 (d, J = 10.7 Hz, $ReCOCH_2$), 191.8 (d, J = 10.7 Hz, ReCO), 191.7 (d, J = 10.7 Hz, ReCO), 190.4–189.6 (nine lines, ReCO for both **5** and **5**-OH), 136.6–130.5 (m, C_6H_5 for both **5** and **5**-OH), 128.9 (d, J = 9.9 Hz, C_6H_5), 102.7 (d, J = 1.5 Hz, $C_5(CH_3)_5$), 102.4 (br s, CH_2), 18.0 (d, J = 33.6 Hz, $P(CH_3)_3$), 10.0 ($C_5(CH_3)_5$); for **5**-OH δ 249.3 (d, J = 9.2 Hz, $ReCOCH_2$), 195.1 (dd, J = 12.6, 5.0 Hz, ReCO), 141.0 (m, =CH—), 128.7 (d, J = 9.8 Hz, C_6H_5), 102.0 (d, J = 1.5 Hz, $C_5(CH_3)_5$), 18.0 (d, J = 33.6 Hz, $P(CH_3)_3$), 9.9 ($C_5(CH_3)_5$). Anal. Calcd for $C_{38}H_{41}NO_7P_2Re_2$: C, 43.14; H, 3.91. Found: C, 43.39; H, 3.86. A sample of **5** was recrystallized from ether/hexanes at −20 °C, yielding clumps of red and orange crystals which could be separated by hand. The red crystals contained predominantly **5**-OH (29 mg, [**5**-OH]/[**5**] = 2.9), while the orange crystals contained predominantly **5** (89 mg, [**5**-OH]/[**5**] <0.02) by ^{1}H NMR spectroscopy ($CDCl_3$). Solutions of the red crystals (10.9 mg, 26 mM; THF-d_8, 0.39 mL) and of the orange crystals (13.2 mg, 28 mM; THF-d_8, 0.45 mL) were allowed to stand for 1 week, establishing K_{eq} = 0.65 ([**5**-OH]/[**5**]).

X-ray Crystal Structure Determinations for $(\eta^5$-$C_5Me_5)(NO)(PPh_3)$-$Re[\mu$-$(COCH_2CO)$-C^1:$C^3]Re(PMe_3)(CO)_4$ (5) and $\{(\eta^5$-$C_5Me_5)(NO)$-

$(PPh_3)Re[\mu$-(COCHCOH)-C^1:C^3]$Re(CO)_4(PMe_3)$] (5-OH). X-ray data were collected on a Nicolet R3m/V automated diffractometer system with a dedicated MicroVAX II computer system. Suitable crystals for both compounds were cocrystallized from diffusion of hexanes into a toluene solution and were sealed in glass capillaries under nitrogen. The parameters used during collection of diffractometer data for complexes **5** and **5-OH** are summarized in Table III. No systematic variation in intensities of three standard reflections for either data set were noted. All computations used the SHELXTL PLUS (Version 4.11) program library (Siemens Corp., Madison, WI). For **5**, the initial choice of the centrosymmetric space group $P\bar{1}$ was confirmed by the successful solution and refinement of the structure.

Both structures were solved by direct methods and subsequent Fourier syntheses located all non-hydrogen atoms. All hydrogen atoms were placed isotropically in idealized positions. Although both the Re(1) unit and malonyl bridge of **5-OH** are well-behaved, excessive thermal parameters and distortion of the carbonyl positional parameters in the Re(2) unit suggested a mild disorder problem. Because of this, the carbonyl ligands were placed as rigid groups with fixed isotropic thermal parameters. All other non-hydrogen atoms except the phenyl carbons were refined anisotropically. The final Fourier difference map revealed a residual electron density peak of 2.87 e, 1.06 form Re(2). For **5**, all non-hydrogen atoms except C(42) and C(6) and the phenyl carbons were refined anisotropically. No excessive thermal motion was noted in this structure; however, uncompensated absorption from the thin plate used for data collection resulted in pairs of residual electron density peaks of 1.47-3.69 e, symmetrically placed about the Re(1) and Re(2) centers.

Acknowledgment. Partial support of the National Science Foundation (CHE-9005973) is gratefully acknowledged. The NMR spectrometer utilized was acquired via NIH and NSF instrumentation Grants RR04733 and CHE-8814866.

Supplementary Material Available: Listings of fractional coordinates, bond distances, bond angles, hydrogen atom coordinates, and thermal parameters for **2**-Re-OSi, **2**-Mn-OSi, **5**, and **5-OH** (22 pages); tables of observed and calculated structure factors (86 pages). Ordering information is given on any current masthead page.

Gas-Phase Heteroaromatic Substitution. 12.[1] Reaction of Free Trifluoromethyl Cation with Simple Five-Membered Heteroarenes in the Gas Phase

Roberto Bucci,[†] Giuseppe Laguzzi,[†] Maria Luisa Pompili,[†] and Maurizio Speranza*,[‡]

Contribution from the Istituto di Chimica Nucleare del CNR, Area della Ricerca di Roma, Rome, Italy, and the Dipartimento di Agrobiologia ed Agrochimica, Università della Tuscia, Viterbo, Italy. *Received July 26, 1990. Revised Manuscript Received January 21, 1991*

Abstract: The reactivity features of radiolytically (^{60}Co γ-rays) generated unsolvated trifluoromethyl cation CF_3^+ toward pyrrole, *N*-methylpyrrole, furan, and thiophene have been measured under conditions, i.e. 7 Torr of C_2H_4 added, ensuring depletion of concomitant radicalic processes. Experiments have been carried out at atmospheric pressure and in the presence of variable concentrations of a gaseous base (NMe_3, 0-5 Torr). The mechanism of the ionic trifluoromethylation process and of the subsequent isomerization of the relevant ionic intermediates is discussed and the intrinsic positional selectivity of CF_3^+ ions evaluated. The preference of CF_3^+ for the β carbons of pyrroles (ca. 56%) and furan (ca. 78%) and the α carbons of thiophene (ca. 59%) conforms to a substitution route proceeding via the classical donor-acceptor S_E2 mechanism, ruling out alternative substitution pathways, including the two-step process advanced in the case of gas-phase acylation of the same substrates. The selectivity features of the CF_3^+ ion toward pyrroles appear to fit into Klopman's reactivity model, since determined essentially, but not exclusively, by its LUMO energy. The pronounced preference of CF_3^+ toward the β carbons of furan is discussed and compared with the general tendency of other gaseous alkyl carbocations, irrespective of their LUMO energy, to attack predominantly the α carbons of the same substrate. It is concluded that such a tendency is due to the establishment of electrostatic interactions between the n-electrons of the oxygen of furan and the hydrogens of the alkylating electrophile, a process which is prevented in the case of CF_3^+.

Introduction

The essence of Klopman's charge and frontier orbital control concept[2] in a donor-acceptor reaction is that, when the energy gap between the HOMO of the donor and the LUMO of the acceptor is small compared to that between the orbitals of the individual reagents, the reaction is "frontier-orbital controlled", i.e. it is governed by bonding between the atoms carrying the highest charge density in the frontier orbitals. When, instead, the energy gap between the HOMO of the donor and the LUMO of the acceptor progressively increases, the reaction tends to be "charge controlled", i.e. it is regulated by attractive electrostatic interactions between the centers of the two reagents with the highest total charge. If the acceptor is a free, unsolvated ionic electrophile and the donor is a five-membered heteroarene, such as pyrrole and furan, having a HOMO electron density distribution opposite to the total charge-density one,[3] a detailed investigation of their reactivity and selectivity features may represent a powerful means for ascertaining whether Klopman's model is actually adequate for describing heteroaromatic reactivity, especially if the study is carried out in the gas phase, where solvation and ion-pairing factors normally affecting the intrinsic reactivity properties of both the donor and the acceptor are excluded.

In recent years, intense research effort has been actually channelled in this direction.[1,4] The study allowed for the es-

[†] Istituto di Chimica Nucleare del CNR.
[‡] University of Tuscia.

(1) Part 11: Filippi, A.; Occhiucci, G.; Sparapani, C.; Speranza, M. *Can. J. Chem.* In press.
(2) (a) Klopman, G. *J. Am. Chem. Soc.* **1968**, *90*, 223. (b) Pearson, R. G. *Proc. Natl. Acad. Sci. U.S.A.* **1986**, *83*, 8440.
(3) Speranza, M. *Adv. Heterocycl. Chem.* **1986**, *40*, 25.
(4) (a) Speranza, M. *J. Chem. Soc., Chem. Commun.* **1981**, 1177. (b) Angelini, G.; Sparapani, C.; Speranza, M. *J. Am. Chem. Soc.* **1982**, *104*, 7084. (c) Angelini, G.; Lilla, G.; Speranza, M. *J. Am. Chem. Soc.* **1982**, *104*, 7091; (d) Margonelli, A.; Speranza, M. *J. Chem. Soc., Perkin Trans. 2* **1983**, 1491. (e) Angelini, G.; Laguzzi, G.; Sparapani, C.; Speranza, M. *J. Am. Chem. Soc.* **1984**, *106*, 37. (f) Laguzzi, G.; Speranza, M. *J. Chem. Soc., Perkin Trans. 2* **1987**, 857. (g) Angelini, G.; Sparapani, C.; Speranza, M. *J. Am. Chem. Soc.* **1990**, *112*, 3060. (h) Laguzzi, G.; Bucci, R.; Grandinetti, F.; Speranza, M. *J. Am. Chem. Soc.* **1990**, *112*, 3064. (i) Crestoni, M. E.; Fornarini, S.; Speranza, M. *J. Am. Chem. Soc.* **1990**, *112*, 6929. (j) Filippi, A.; Occhiucci, G.; Speranza, M. *Can. J. Chem.* In press.

0002-7863/91/1513-4544$02.50/0